

High Energy Density Physics (HEDP) And Laboratory Astrophysics



Associate Professor Louise Willingale



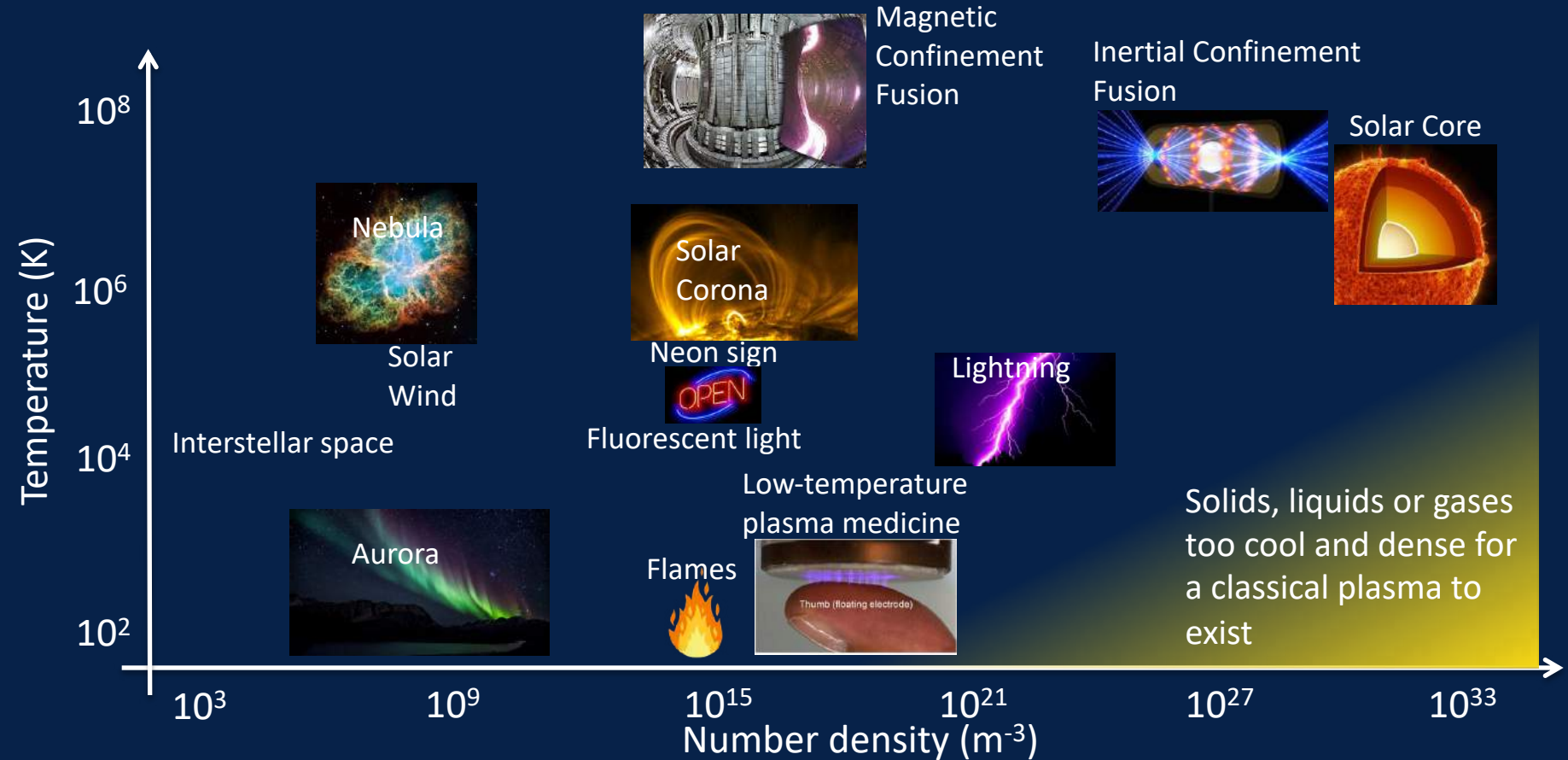
COLLEGE OF ENGINEERING
ELECTRICAL & COMPUTER ENGINEERING
UNIVERSITY OF MICHIGAN

GPAP 2023, 31st May 2022

HEDP and Laboratory Astrophysics

- What is HEDP?
- Creating HEDP conditions in the laboratory
 - Z-pinch (pulsed power machines)
 - High-energy laser facilities
- Examples of astrophysically relevant HEDP experiments
 - Equation of state, stellar opacity, nuclear cross-sections, turbulent dynamo, instabilities (Rayleigh-Taylor, Weibel), scaled protostellar jets
- Magnetic reconnection in the laboratory
- Pair plasmas in the laboratory?
- Extreme plasmas in the laboratory?

Plasma conditions



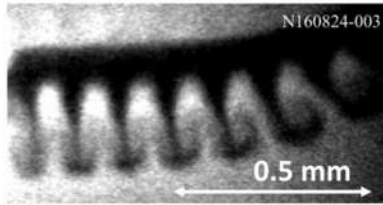
Laboratory Plasma Physics to Astrophysics

Micro-plasma processes in laboratory



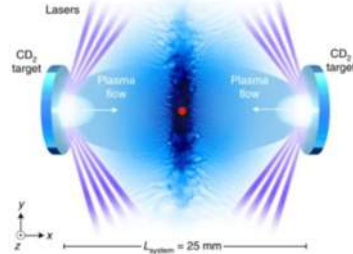
Macro-plasma processes on astro-scales

Instabilities



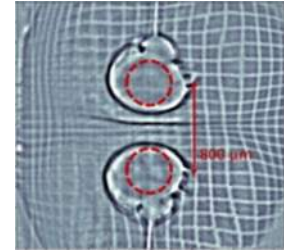
Remington, PNAS (2018)

Collisionless Shocks



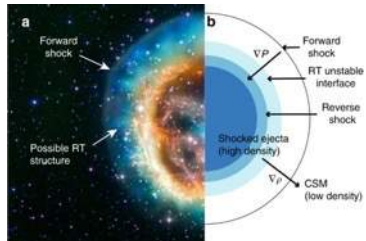
Fiuza, Nature Physics (2020)

Magnetic Reconnection



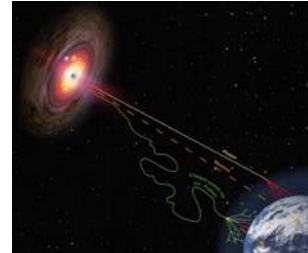
Tubman, Nature Comms (2021)

Supernova remnants



Kuranz, Nature Comms (2018)

Cosmic ray origin



credit: HAP / A. Chantelauze

Solar flares



NASA's Solar Dynamics Observatory

What is High Energy Density Physics (HEDP)?

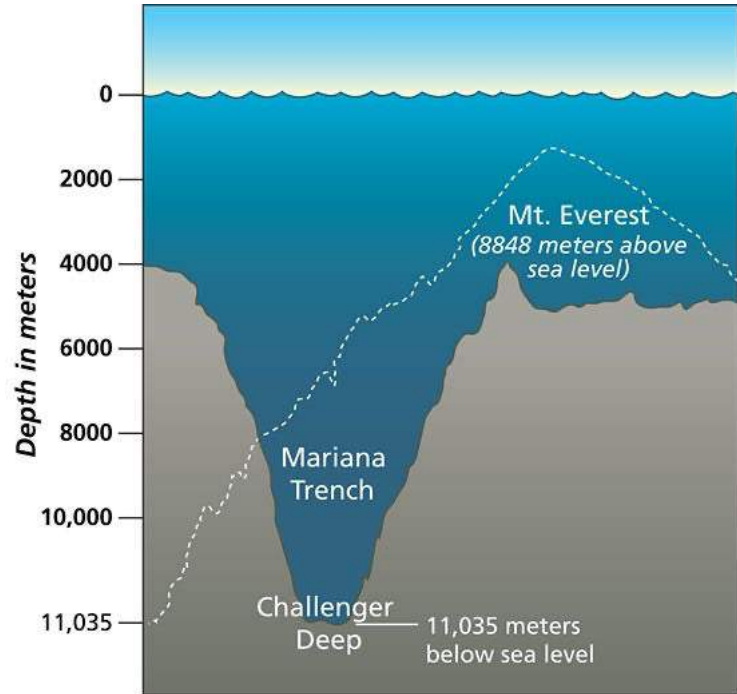
- Pressure above 1 Mbar = 1 million atm
- ~ Boeing 747 on your fingertip



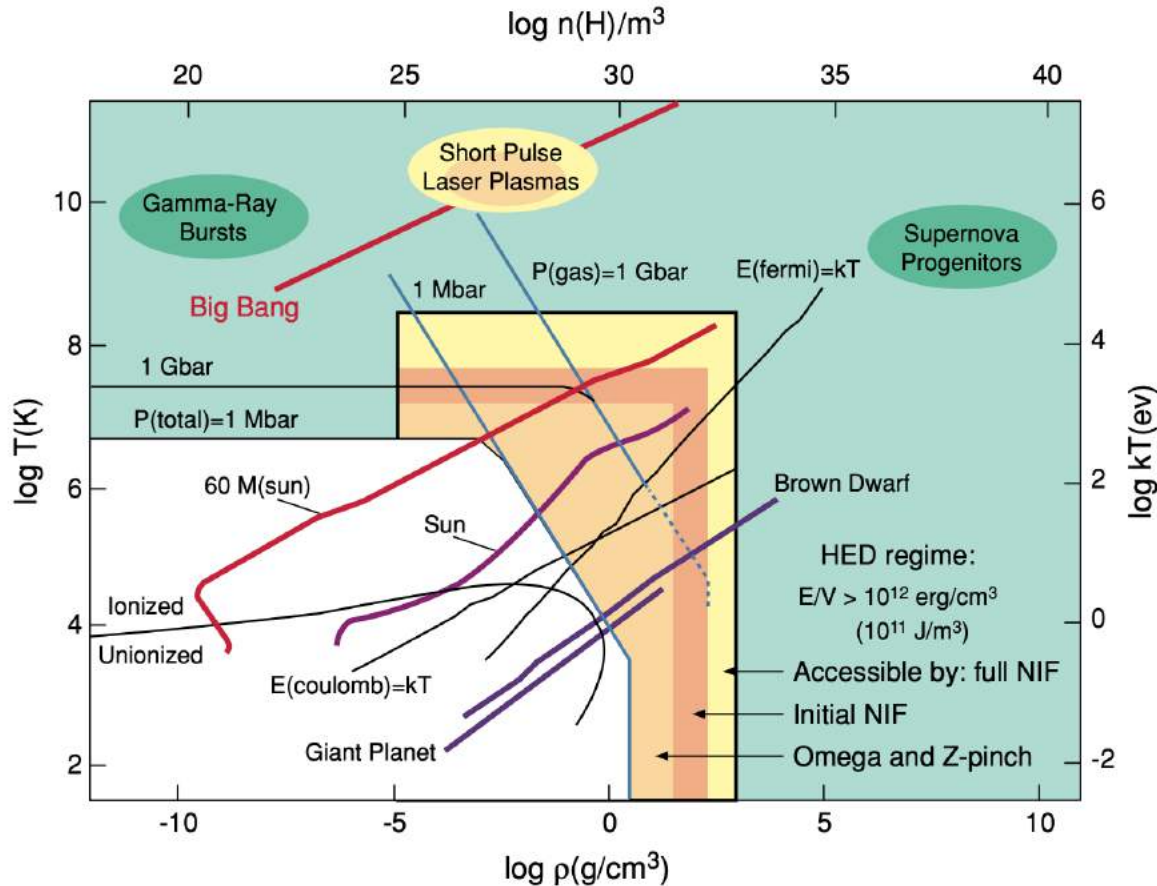
$$P = \frac{F}{A}$$

1000 atm →

- In the ocean, reach
 - 1 atm at 10 m
 - 1 Mbar at 10^6 m (10 million meters)



What is HEDP?



1 eV \sim 10,000 K

1 MeV \sim 10^{10} K

- At high density, get pressure ionization
- The lines for $P = 1\text{ Mbar}$, etc indicate the T_e at which an equilibrium radiation field produces these pressures
- Strongly coupled: to the right of the line $E(\text{Coulomb}) = kT$, energy of Coulomb interactions exceeds the thermal energy

[Frontiers in High Energy Density Physics: The X-Games of Contemporary Science, National Research Council \(2003\)](#)

What is HEDP?

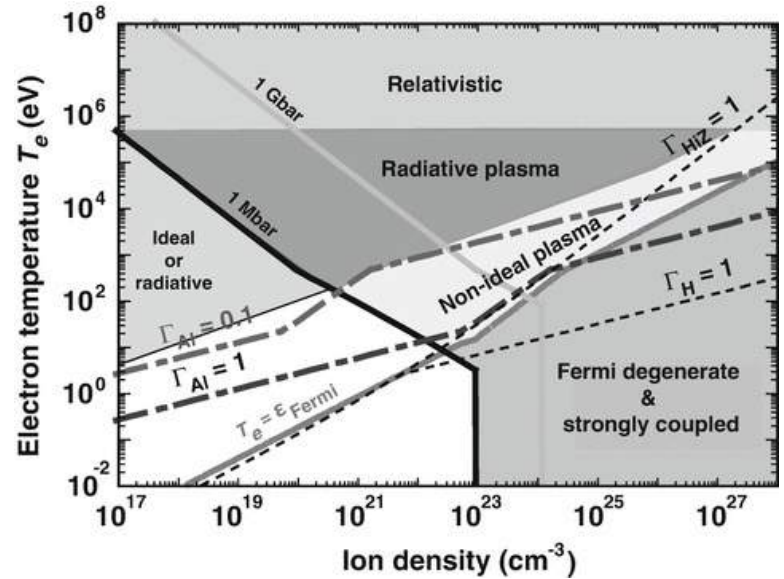
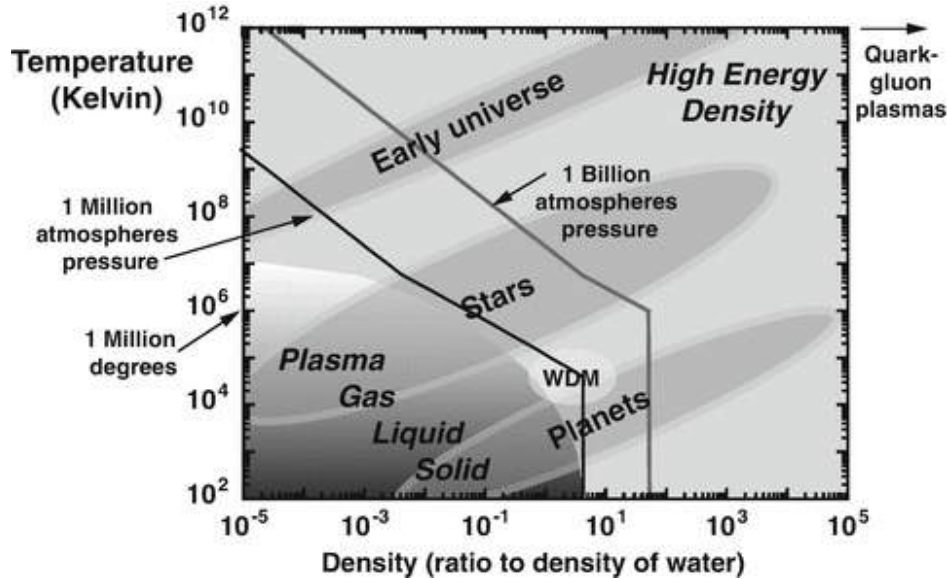
- Fermi degenerate: to the right of the line $E(\text{Fermi}) = kT$, the Fermi energy exceeds the thermal energy
- # of electrons in a Debye sphere:

$$\Lambda = 4\pi n_e \lambda_D^3$$

$$\lambda_D^2 = \frac{\epsilon_0 k_B T_e}{n_e e^2} \quad \rightarrow \quad \Lambda = 4\pi \epsilon_0 \frac{(k_B T_e)^{3/2}}{n_e^{1/2}}$$

- If Λ is small \rightarrow non-ideal plasma
- For HED matter, it's typically a plasma, but plasma theory may not be sufficient

High Energy Density Physics



R P Drake, (2018) Introduction to High-Energy-Density Physics, Graduate Texts in Physics. Springer, Cham. https://doi.org/10.1007/978-3-319-67711-8_1

Why study HEDP?

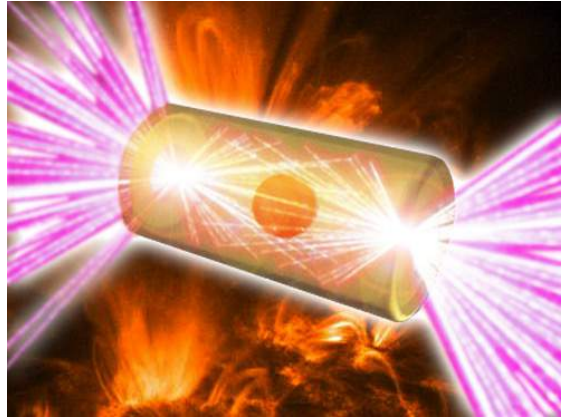
National Nuclear Security Association

Science-based stockpile stewardship to ensure a safe, secure, and effective nuclear stockpile



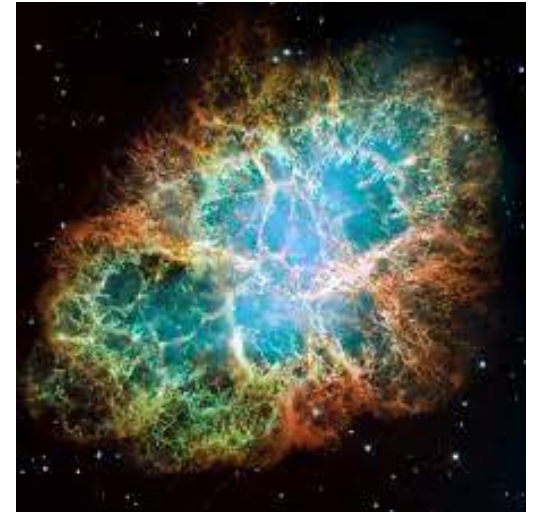
Inertial Confinement Fusion Scientists

Create nuclear fusion reactions by heating and compressing a fuel



Astrophysicists

HEDP conditions found in SN explosions, SN remnants, accretion phenomena, reconnection, cosmic ray acceleration...



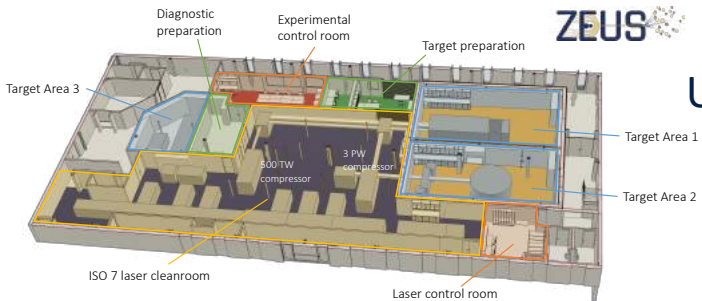
Creating HEDP conditions

High-energy, short pulse lasers



National lab scale

Z-pinch

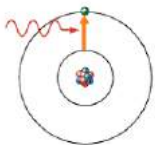


University scale



Time scales

Atomic processes

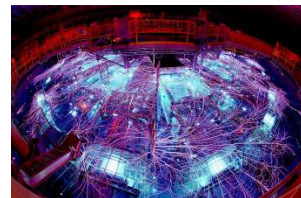
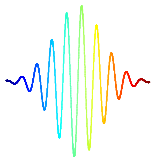


30 fs
Ti:Sapph
CPA lasers

~ 1 ps
Nd:glass
CPA lasers

20 ns
NIF,
OMEGA

< 100 ns
Z-pinch
currents



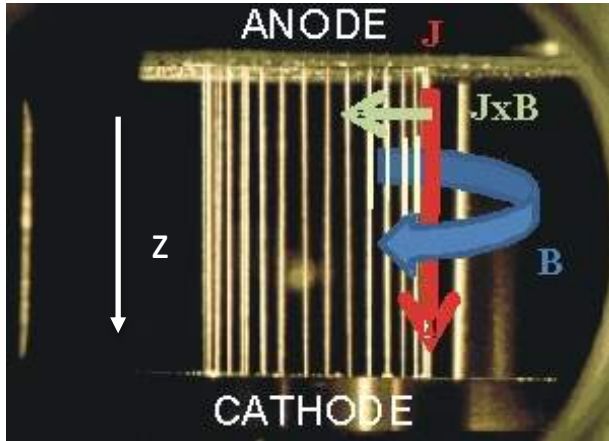
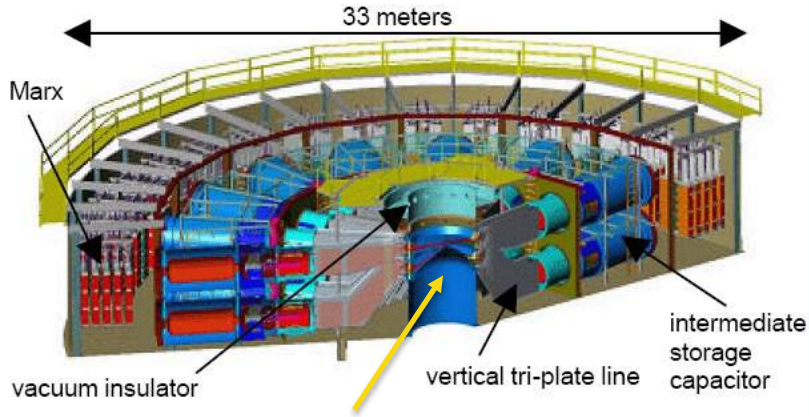
attosecond
as
 10^{-18} s

femtosecond
fs
 10^{-15} s

picosecond
ps
 10^{-12} s

nanosecond
ns
 10^{-9} s

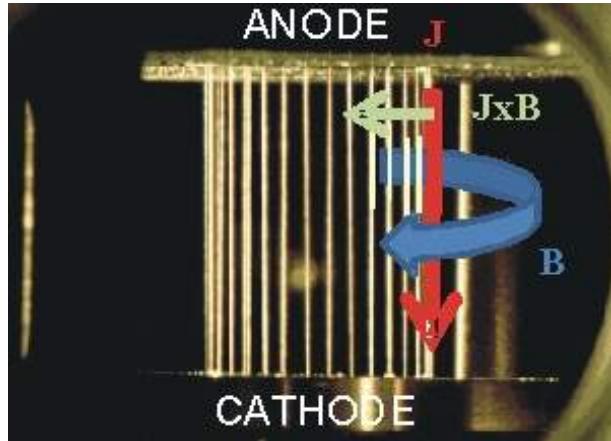
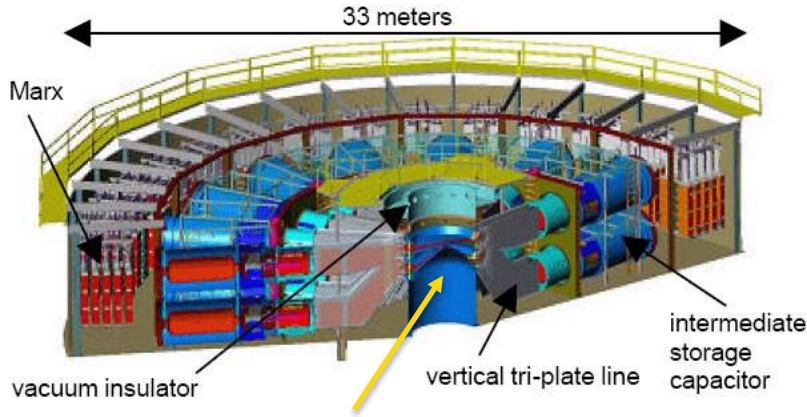
Creating HEDP conditions: Z-pinch



Wire array

Wires are heated by the current, and ablate plasma

Creating HEDP conditions: Z-pinch

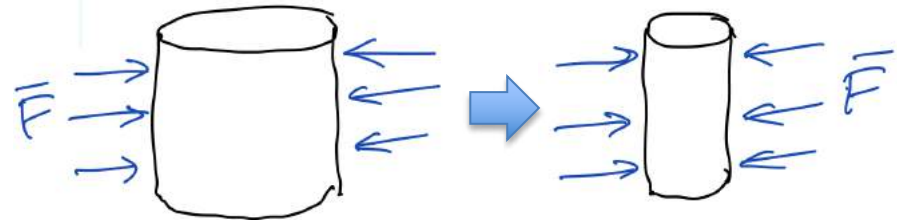


Wire array

Force on the plasma due to magnetic pressure (Lorentz force)

$$\bar{F} = \frac{\bar{J} \times \bar{B}}{v} = -P_{mag} 2\pi R h$$

Where R = radius and h = height



- Assemble dense, hot plasma on axis
- Source of bright x-rays
- Instabilities: sausage, kink, magneto RT

Creating HEDP conditions: Laser pulses



[NIF](#) at LLNL

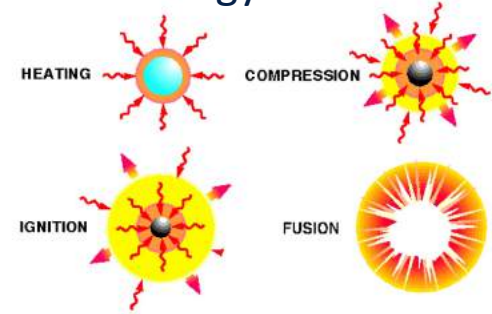


Aka “The Warp Core” on StarTrek

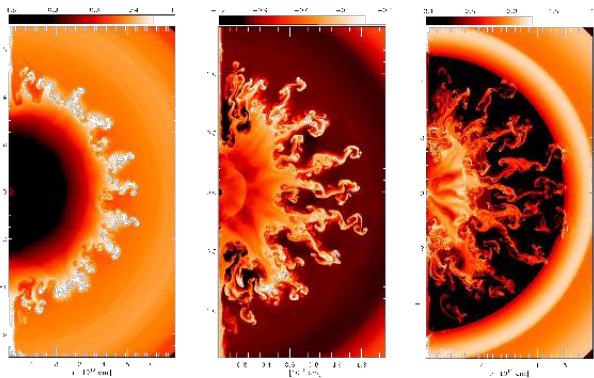
What can these facilities study?

...planetary interiors, equation of state, atomic processes, radiation transport, photoionization, stellar opacity, magnetic reconnection, particle acceleration, collisionless plasmas, turbulent dynamos, nuclear astrophysics, pair plasmas...

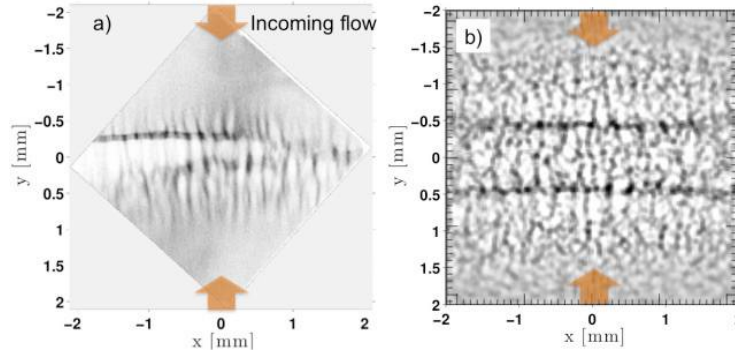
Fusion energy studies



Basic plasma instabilities



Fundamental & nuclear physics



Equation of state



Target plasma density

If the laser frequency, ω_L , equals the electron plasma frequency

$$\omega_L = \omega_{pe} = \sqrt{\frac{n_e e^2}{\epsilon_0 m_e}}$$

then the critical density is found:

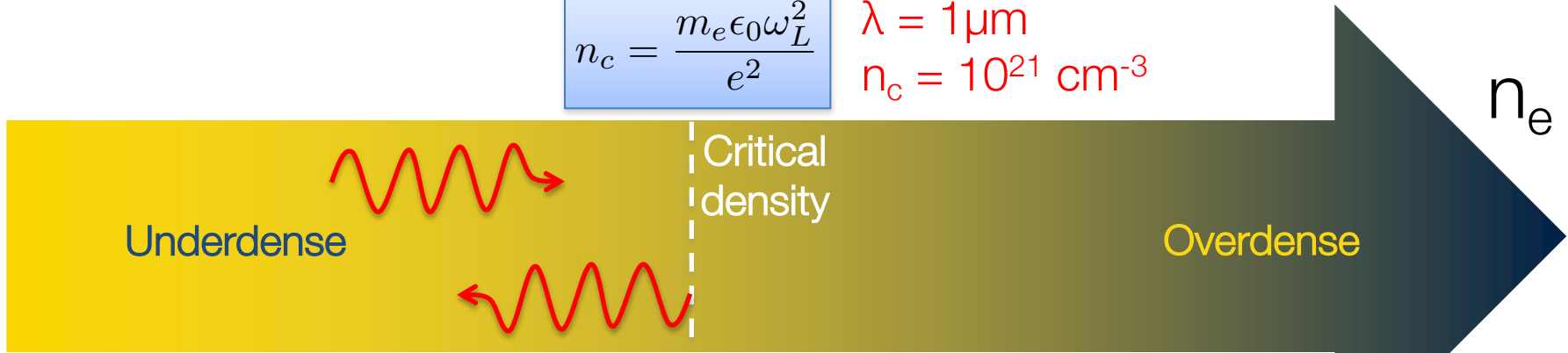
$$n_{cr} = \frac{m_e \epsilon_0 \omega_L^2}{e^2}$$

Target plasma densities

$$n_c = \frac{m_e \epsilon_0 \omega_L^2}{e^2}$$

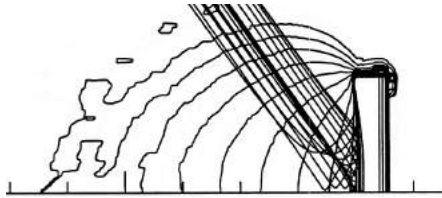
$$\lambda = 1 \mu\text{m}$$

$$n_c = 10^{21} \text{ cm}^{-3}$$

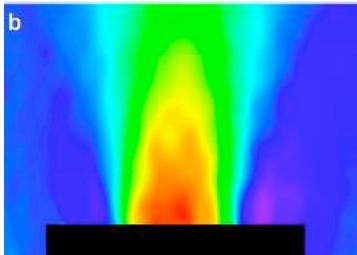


Gas Jet
 $10^{18} - 10^{20} \text{ cm}^{-3}$

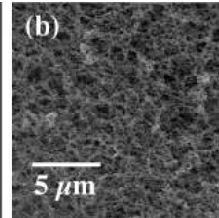
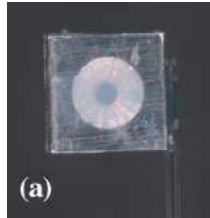
Plasma plume



Solid foil $\sim 10^{24} \text{ cm}^{-3}$



Foam
 $0.9 - 30 \times 10^{21} \text{ cm}^{-3}$



Blackbody radiation

Hot material radiates energy as photons

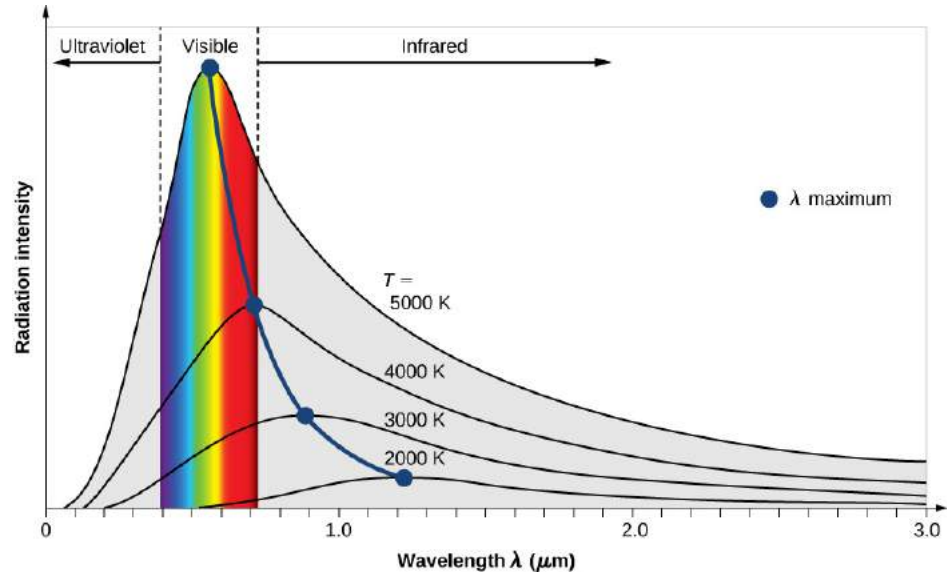
Blackbody radiation spectrum is given by Planck's law:

spectral radiance (power / unit solid angle / unit area normal to propagation) density of frequency, ν , radiation per unit frequency at thermal equilibrium at temperature T ,

$$B_{\nu}(T) = \frac{2h\nu^3}{c^2} \frac{1}{e^{h\nu/kT} - 1}$$

Planck constant, $h = 6.6 \times 10^{-34} \text{ Js} = 4.1 \times 10^{-15} \text{ eV.s}$

Blackbody radiation is isotropic

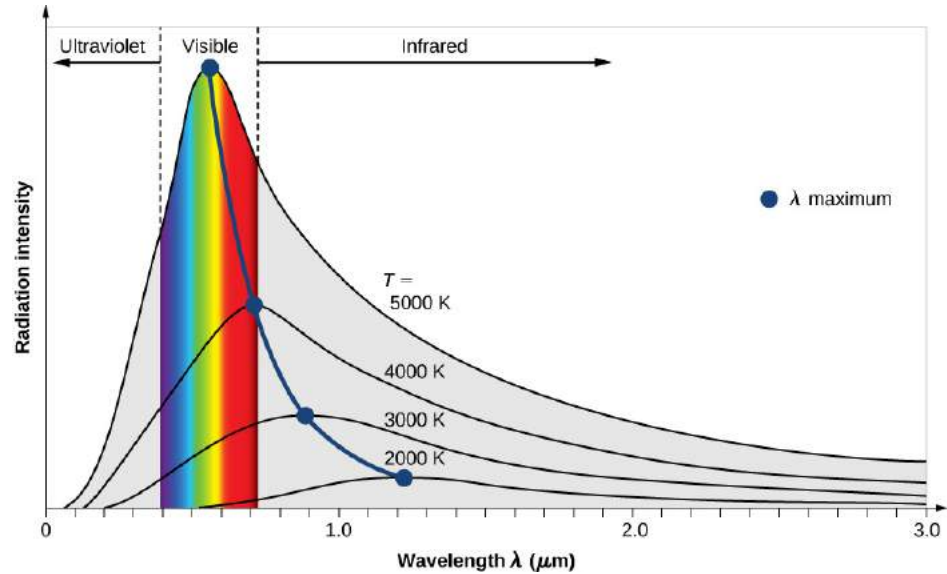


Higher T :

- Peak shifts to lower λ (higher photon energy)
- Radiation intensity increases

Blackbody radiation

- We can use laser pulses to heat materials to high temperatures
- The material will then radiate a blackbody spectrum...



Higher T:

- Peak shifts to lower λ (higher photon energy)
- Radiation intensity increases

Radiation hydrodynamics

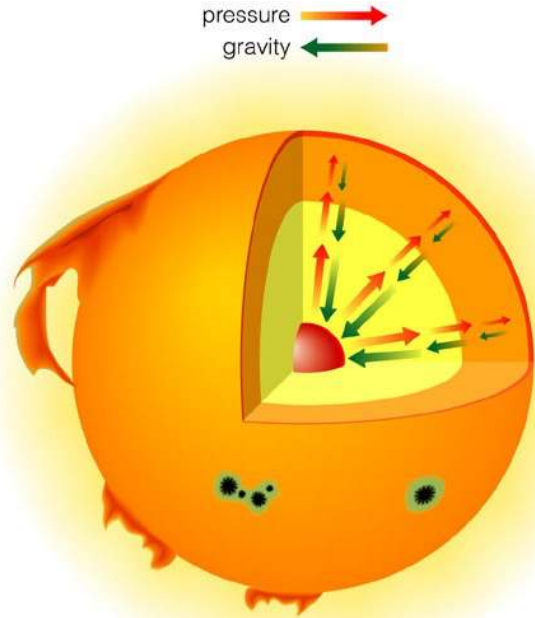
- Plasma gains or loses energy and momentum through photon emission, absorption, and/or scattering.
- This modifies the fluid energy equation and can alter hydrodynamics
- Radiation flux is given by σT^4 (Stefan-Boltzmann Law)
- The radiation hydrodynamics regime is affected by the material, the density and temperature.
- If radiation flux > material energy flux, then it's a radiation dominated regime

Radiation effects

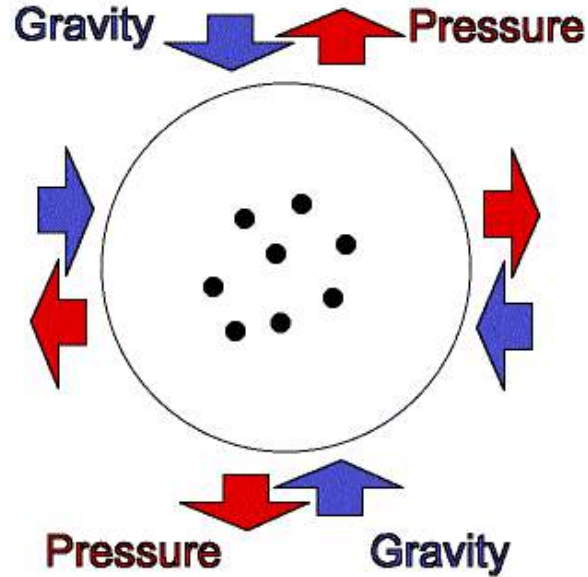
Fluid effects

We can drive experiments with blackbody radiation

Creating a star on Earth



pressure →
gravity ←



Thermonuclear fusion heats the inside of the star, creating pressure that stops the collapse and producing a long period of great stability that defines the main sequence

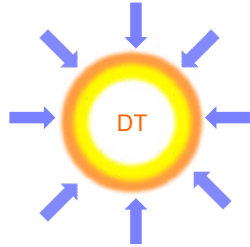
Inertial Confinement Fusion (ICF)

→ Radiation

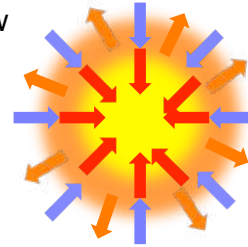
→ Blow-off

→ Inward transported thermal energy

1. Laser beams or laser-produced x-rays rapidly heat the surface of the fusion target, forming a surrounding plasma envelope



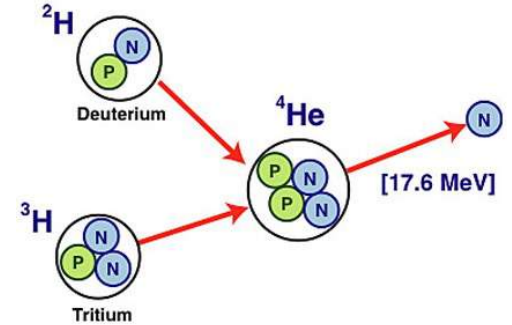
2. Fuel is compressed by the rocket-like blow off of the hot surface material



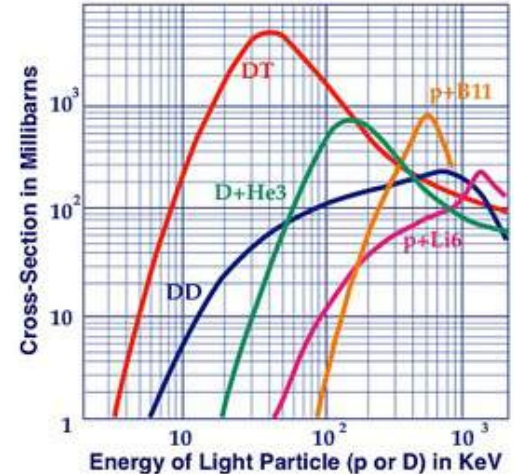
3. During the final part of the capsule implosion, the fuel core reaches 20 times the density of lead and ignites at 100,000,000°C



4. Thermonuclear burn spreads rapidly through the compressed fuel, yielding many times the input energy



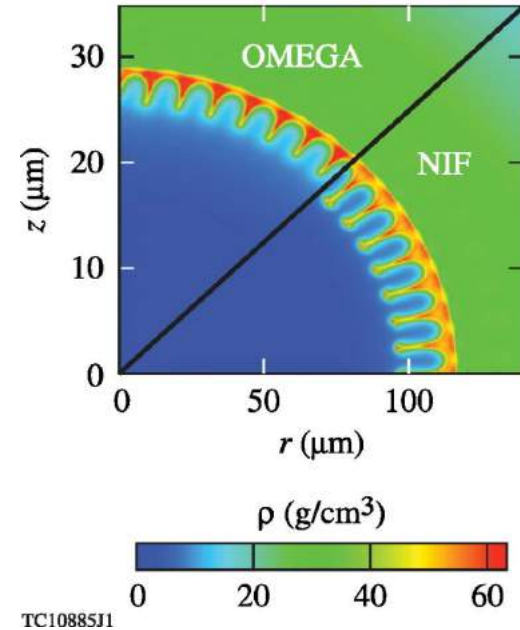
Fusion Reaction Cross-Sections
Particles Have Equal Momentum



Inertial Confinement Fusion

- Hot spot conditions:
- How dense? ~ 100x solid lead
(600 – 800 g/cc)
- How hot? > 100 million K
- How long? ~ 10 ns

Rayleigh-Taylor instability



Equation of State

Article

A measurement of the equation of state of carbon envelopes of white dwarfs

<https://doi.org/10.1038/s41586-020-2535-y>

Received: 12 July 2019

Accepted: 5 May 2020

Published online: 5 August 2020

 Check for updates

Andrea L. Kritcher^{1,2}, Damian C. Swift¹, Tilo Döppner¹, Benjamin Bachmann¹, Lorin X. Benedict¹, Gilbert W. Collins^{1,2,3,4}, Jonathan L. DuBois⁵, Fred Elsner⁶, Gilles Fontaine^{6,14}, Jim A. Gaffney¹, Sebastien Hamel¹, Amy Lazicki¹, Walter R. Johnson⁷, Natalie Kostinski¹, Dominik Kraus^{3,9}, Michael J. MacDonald¹, Brian Maddox¹, Madison E. Martin¹, Paul Neumayer¹⁰, Abbas Nikroo¹, Joseph Nilsen¹, Bruce A. Remington¹, Didier Saumon¹¹, Phillip A. Sterne¹, Wendi Sweet⁸, Alfredo A. Correa¹, Heather D. Whitley¹, Roger W. Falcone¹² & Siegfried H. Glenzer¹³

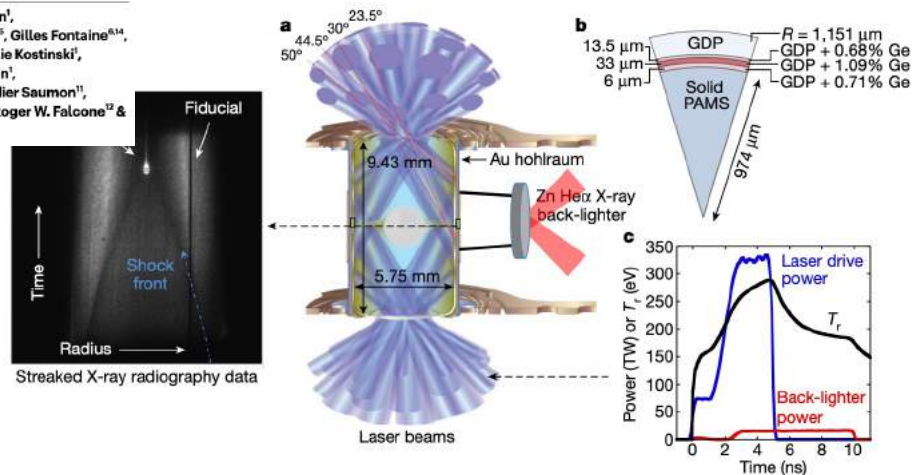


Fig. 1 | Experimental configuration. **a**, Schematic of the target showing laser beams incident on the inside of a gold hohlraum, a solid spherical sample inside the hohlraum, and the X-ray back-lighting configuration. **b**, Diagram of the sample configuration (that is, a portion of the sphere from **a**), showing layer thicknesses and level of Ge dopant (in atoms per cent) in the glow-discharge

polymer (GDP) ablator. **c**, Laser drive (blue) and back-lighter (red) power profiles versus time. The calculated radiation temperature versus time is also shown (black curve). **d**, Streaked X-ray radiography data showing the shock front and shock flash at the core. The spatial fiducial line is used for diagnostic warp correction.

Equation of State

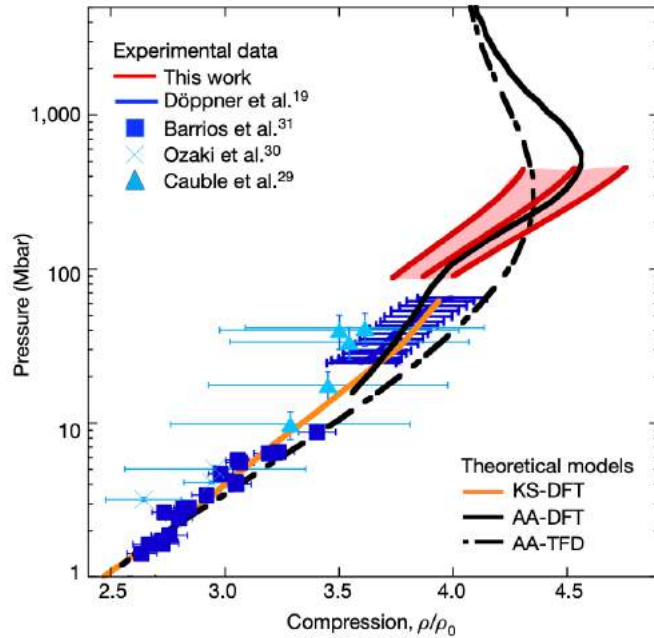


Fig. 3 | $C_v(H)_{10}$ shock Hugoniot measurements. Measured pressure versus mass density (ρ) normalized to the initial density (ρ_0) along the shock Hugoniot (red curve and shaded region). Also plotted are previous experimental data^{19,29–31} and theoretical modelling of the Hugoniot using AA-TFD (black dashed curve), AA-DFT (black curve) and KS-DFT (orange curve); see text.

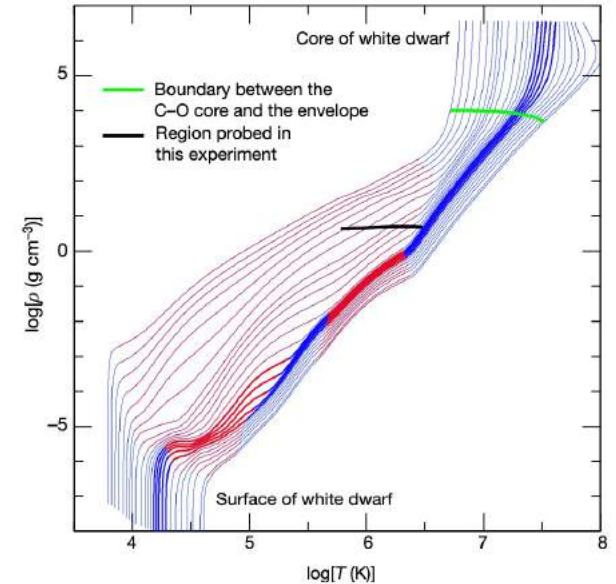
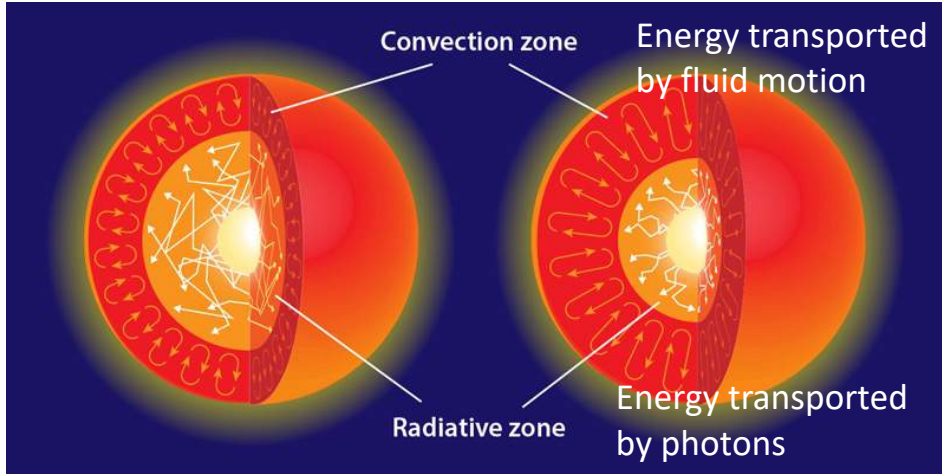


Fig. 4 | Regime of white dwarf stars accessed by measurements. Density–temperature diagram for the evolution of a white dwarf star with a mass of $0.6M_{\text{Sun}}$ composed of a carbon/oxygen core surrounded by a pure carbon envelope (M_{Sun} , mass of the Sun). The surface of the star occupies the region of the curves in the lower left and the core occupies the region of the curves in the upper right. Models start from hot and young state (right) and evolve leftward to older and colder structures, with the bold lines corresponding to hot DQ stars³. Convective regions in the stars are shown in red. The regime probed by the experiment is shown by the thick black line, with temperatures estimated from a model EOS^{33–35}.

Stellar opacity



Processes:

- Bound-bound absorption
- Bound-free absorption
- Free-free absorption
- Electron-scattering

} Single
macroscopic
quantity...

Fusion releases energy:
Particle kinetic energy or photons

Opacity κ is the ability of a material to absorb radiation at each ν

$$\kappa_\nu = \kappa_\nu(\rho, T, X_i)$$

Opacity appears in the energy transport equation.

Mean-free-path: $\ell = \frac{1}{\kappa_\nu \rho}$

Stellar Opacity

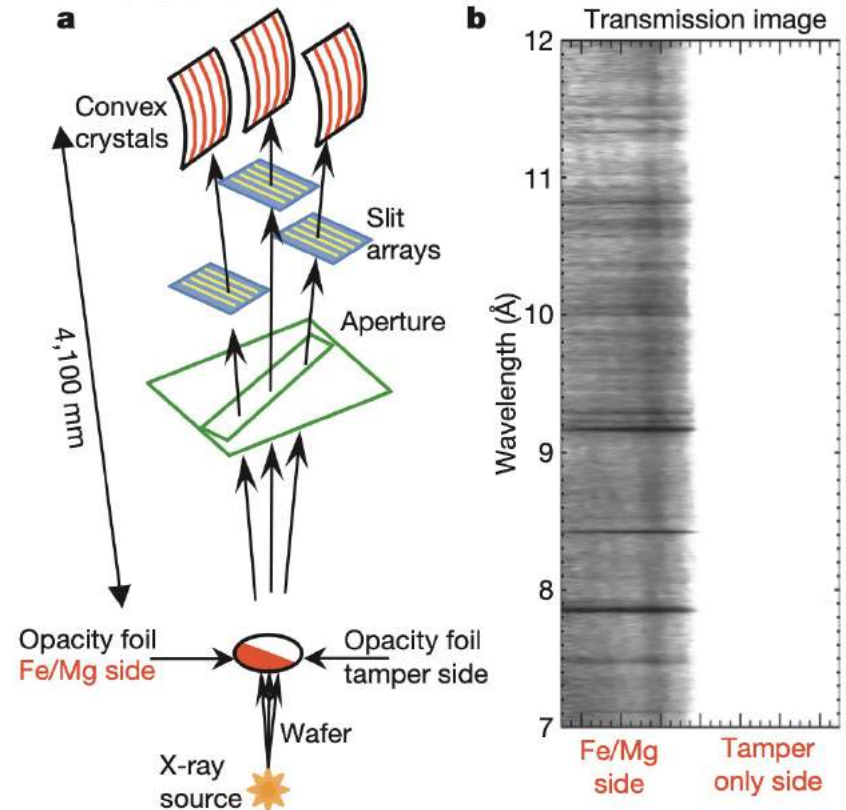
LETTER

doi:10.1038/nature14048

A higher-than-predicted measurement of iron opacity at solar interior temperatures

J. E. Bailey¹, T. Nagayama¹, G. P. Loisel¹, G. A. Rochau¹, C. Blancard², J. Colgan³, Ph. Cosse², G. Faussurier², C. J. Fontes³, F. Gilleron², I. Golovkin⁴, S. B. Hansen¹, C. A. Iglesias⁵, D. P. Kilcrease³, J. J. MacFarlane⁴, R. C. Mancini⁶, S. N. Nahar⁷, C. Orban⁷, J.-C. Pain², A. K. Pradhan⁷, M. Sherrill³ & B. G. Wilson²

Figure 1 | Experiment diagram and example transmission image. **a**, Three to four spectrometers view the 'half-moon'-shaped tamped iron/magnesium sample (not to scale). Each uses multiple slits to project spatially resolved images onto a convex crystal that disperses the spectrum before recording on film (not shown). The set-up measures the unattenuated (tamper only) and the attenuated (tamper plus FeMg) spectra in the same experiment. **b**, A spatially resolved and spectrally resolved transmission image is obtained by dividing the attenuated spectral image by the unattenuated image. Darker regions correspond to higher absorption. The white portion of the image corresponds to $\sim 100\%$ transmission.



<https://www.nature.com/articles/nature14048>

Stellar Opacity

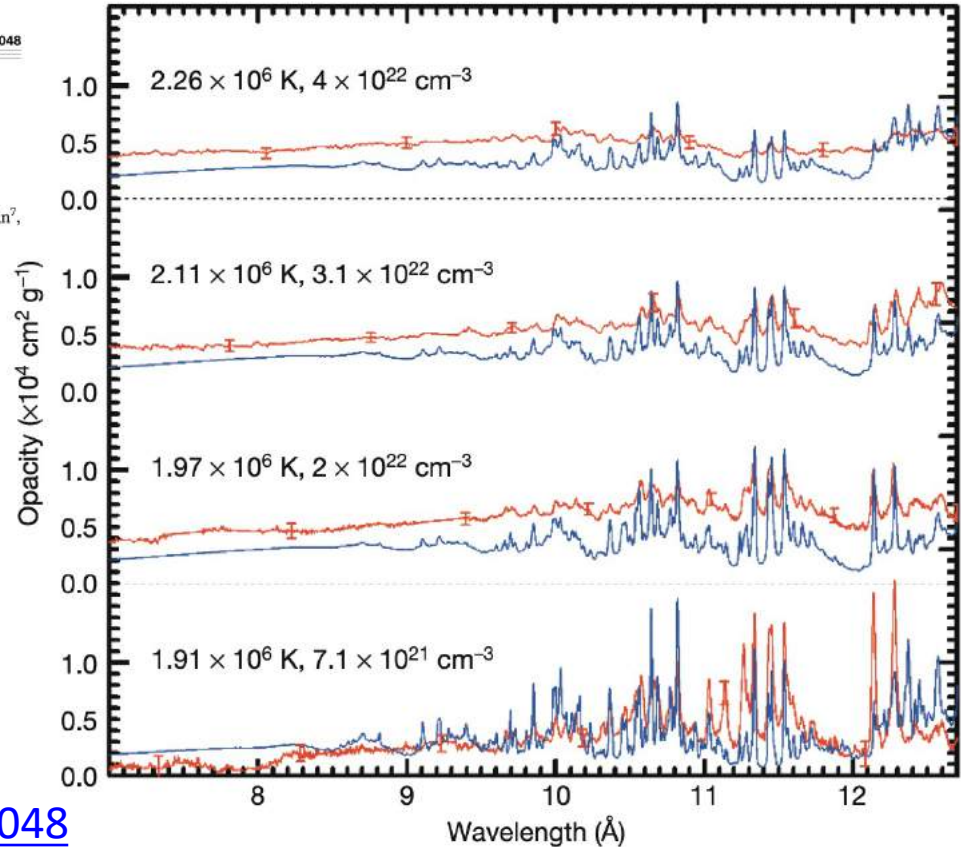
LETTER

doi:10.1038/nature14048

A higher-than-predicted measurement of iron opacity at solar interior temperatures

J. E. Bailey¹, T. Nagayama¹, G. P. Loisel¹, G. A. Rochau¹, C. Blancard², J. Colgan³, Ph. Cosse², G. Faussurier², C. J. Fontes³, F. Gilleron², I. Golovkin⁴, S. B. Hansen¹, C. A. Iglesias⁵, D. P. Kilcrease², J. J. MacFarlane⁴, R. C. Mancini⁶, S. N. Nahar⁷, C. Orban⁷, J.-C. Pain², A. K. Pradhan⁷, M. Sherrill³ & B. G. Wilson²

Figure 2 | Measured iron opacity spectra at four T/n_e values compared with calculations. The SCRAM²³ model calculations (blue lines) account for the instrument resolution. Red lines denote the measurements and the error bars represent 1σ uncertainties. The measurements combine information from 22 separate experiments, each with three or four independent spectrometers that each record 4–6 spectra. The numbers of experiments used to infer the average opacities presented here were as follows: six for the $1.91 \times 10^6 \text{ K}/7 \times 10^{21} \text{ cm}^{-3}$ results; one for the $1.97 \times 10^6 \text{ K}/2 \times 10^{22} \text{ cm}^{-3}$ results; five for the $2.11 \times 10^6 \text{ K}/3.1 \times 10^{22} \text{ cm}^{-3}$ results; and ten for the $2.26 \times 10^6 \text{ K}/4 \times 10^{22} \text{ cm}^{-3}$ results.



<https://www.nature.com/articles/nature14048>

Laboratory scales to astrophysical scales

Microscopic processes:

- Nuclear physics (reaction cross-sections)
- Atomic processes (opacity)
- Equation of state

Macroscopic plasma processes:

- Magnetic reconnection
- Shocks
- Instabilities: Weibel, Rayleigh-Taylor, etc
- Turbulent dynamos
- Particle acceleration
- Pair plasmas

Laboratory scales to astrophysical scales

Identify the relevant dimensionless parameters for the system of interest

- Plasma beta: ratio of the plasma pressure to the magnetic pressure

$$\beta = \frac{n_e k_B T_e}{B^2 / 2\mu_0}$$

- Lundquist number: compares Alfvén crossing timescale to the timescale of resistive diffusion

$$S = \frac{L v_A}{\eta}$$

L = system size

η = magnetic diffusivity

- Reynolds number (how easily particles move around c.f. how quickly momentum is diffused by viscosity)

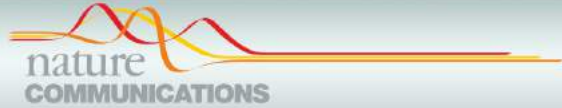
$$R_e = \frac{uL}{\nu}$$

u = characteristic velocity

ν = kinematic viscosity

- Low $R_e \rightarrow$ laminar flow
- High $R_e \rightarrow$ turbulent flow

Plasma instabilities: Rayleigh-Taylor



ARTICLE

DOI: 10.1038/s41467-018-03548-7

OPEN

How high energy fluxes may affect Rayleigh–Taylor instability growth in young supernova remnants

C.C. Kuranz¹, H.-S. Park², C.M. Huntington², A.R. Miles², B.A. Remington², T. Plewa³, M.R. Trantham¹, H.F. Robey², D. Shvarts^{4,5}, A. Shimony^{4,5}, K. Raman², S. MacLaren², W.C. Wan^{1,6}, F.W. Doss⁶, J. Kline⁶, K.A. Flippo⁶, G. Malamud^{1,5}, T.A. Handy¹, S. Prisbrey², C.M. Krauland⁷, S.R. Klein¹, E.C. Harding⁸, R. Wallace², M. J. Grosskopf⁹, D.C. Marion¹, D. Kalantar², E. Giraldez⁷ & R.P. Drake¹

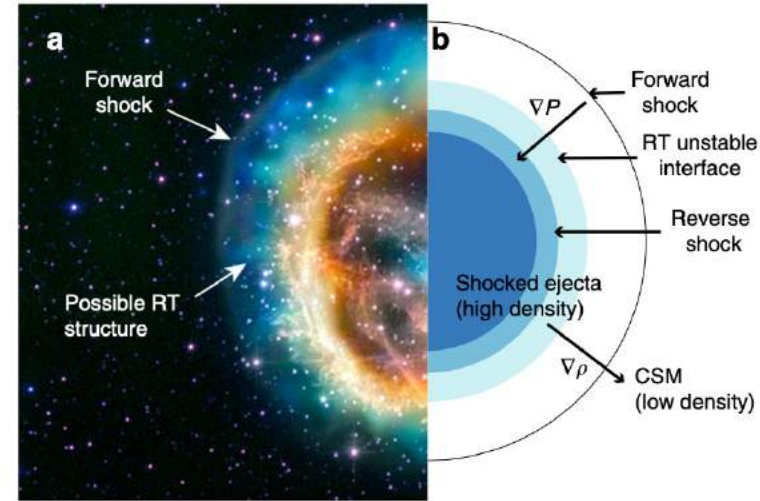
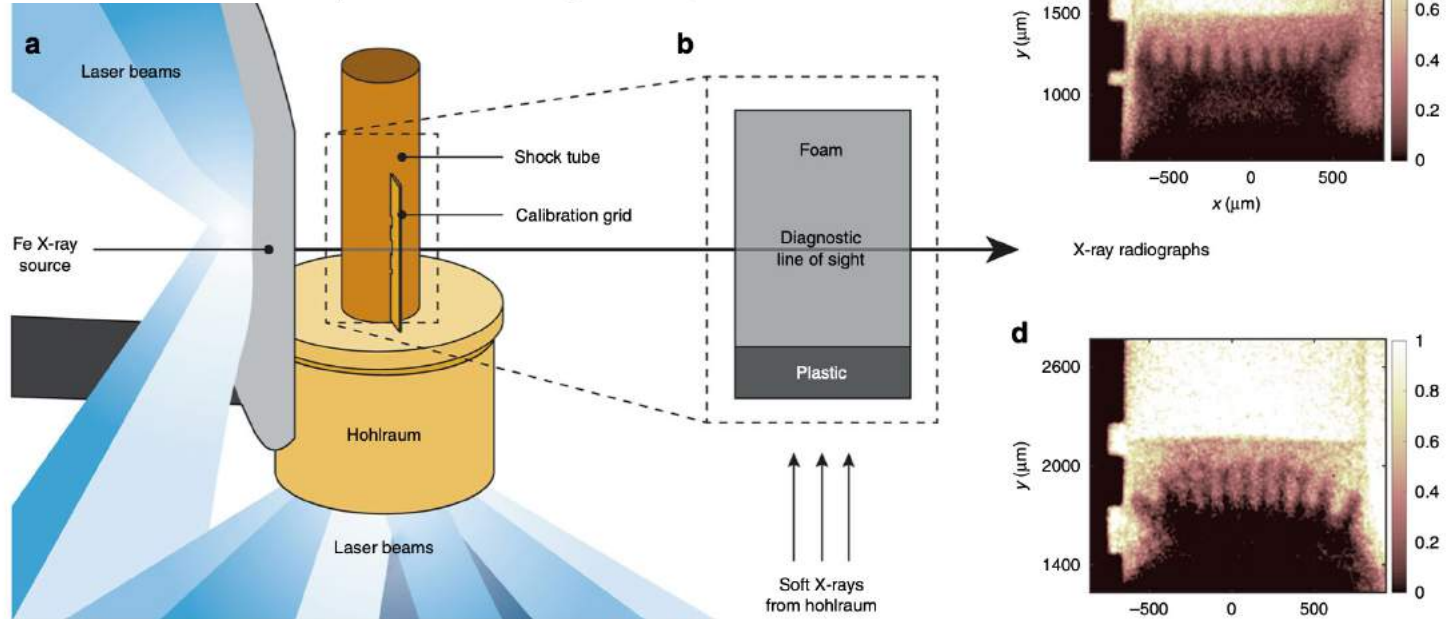


Fig. 4 Image of supernova remnant. **a** False-color image of SNR E0102.2-72. This object is believed to result from a core-collapse supernova about 1000 years ago. One can see the edge of the forward shock. The modulated boundary within it might be structuring of the ejecta-CSM interface produced by RT. The brighter, inner colors are attributed to emission from the higher-Z, interior portions of the ejecta. We credit John Hughes of Rutgers University with having called the potential connection to RT to our attention. Image credit: X-ray (NASA/CXC/MIT/D. Dewey et al. and NASA/CXC/SAO/J. DePasquale); Optical (NASA/STScI). **b** Schematic (size and shape not to scale) of inner structures of the supernova that creates the opposing density and pressure gradients to create an RT unstable interface

Plasma instabilities: Rayleigh-Taylor

Fig. 1 Experimental target and radiographs. **a** NIF target schematic with laser beams incident on the gold hohlraum to create the X-ray drive and on the large-area backlighter to create the diagnostic X-ray source. Attached to the hohlraum is a plastic shock tube. The soft X-rays from the hohlraum create a shock wave in the plastic layer inside the shock tube **b**, which decays into a blast wave before crossing the unstable interface and entering the foam. The diagnostic X-ray source creates radiographs by being preferentially absorbed by a tracer layer in center of the plastic. **c**, **d** X-ray radiographs of the experiment. Here, the plasma flows upward and the dark fingers are due to RT instability growth. The color bar indicates the relative transmission for **c** the high-flux case at $t = 13$ ns and **d** the low-flux case taken at $t = 34$ ns. The two experiments have similar RT growth factors, as described in the text



Plasma instabilities: Rayleigh-Taylor

Scale Parameter	SN1993J	NIF experiment
Intershock distance L (cm)	$2.8 \times 10^{14} t_{\text{yr}}^{0.95}$	0.02
Shock separation speed U (cm $^{-1}$)	$3.0 \times 10^8 t_{\text{yr}}^{-0.046}$	6.8×10^6
Ejecta density at RS (g cm $^{-3}$)	$3.4 \times 10^{-19} t_{\text{yr}}^{-1.6}$	0.026
SEL Density (g cm $^{-3}$)	$1.4 \times 10^{-16} t_{\text{yr}}^{-1.6}$	0.5
SCSM Density (g cm $^{-3}$)	$9 \times 10^{-19} t_{\text{yr}}^{-1.6}$	0.18
SEL Temperature (eV)	$3800 t_{\text{yr}}^{-0.092}$	20
SCSM Temperature (eV)	$7.8 \times 10^5 t_{\text{yr}}^{-0.092}$	80
RS Velocity (km s $^{-1}$)	$1.7 \times 10^4 t_{\text{yr}}^{-0.046}$	35
FS Velocity (km s $^{-1}$)	$2 \times 10^4 t_{\text{yr}}^{-0.046}$	170
Z	1	2
A	1	20

Plasma instabilities: Rayleigh-Taylor

Table 1 Dimensionless parameters and their physical meaning

Dimensionless number	SN1993J	NIF experiment	Physical meaning
λ_c/L	$\sim 10^{-4}$	$\sim 10^{-8}$	Highly collisional
Re	$\sim 10^6$	$\sim 10^7$	Negligible viscosity
Energy flux ratio R	$\sim 10^3$	~ 2	Energy fluxes are important

Both SN1993J (at 0.1 years) and the laboratory experiment have characteristic length $L \gg \lambda_c$, the mean free path for ion-ion collisions, in their denser shocked layers. They also have large Reynolds number, $Re = UL/\nu$, where U is the characteristic velocity and ν is the kinematic viscosity. The text discusses the energy flux ratio R

Reynolds number (how easily particles move around c.f. how quickly momentum is diffused by viscosity)

$$R_e = \frac{uL}{\nu}$$

u = characteristic velocity

ν = kinematic viscosity

Low $R_e \rightarrow$ laminar flow

High $R_e \rightarrow$ turbulent flow

Biermann battery field generation

Ohm's law:

$$\bar{\mathbf{E}} = \underbrace{-\bar{\mathbf{u}} \times \bar{\mathbf{B}}}_{\text{Ideal MHD}} + \underbrace{\frac{\bar{\mathbf{j}}}{\sigma}}_{\text{Resistive MHD}} + \underbrace{\frac{1}{en_e} \bar{\mathbf{j}} \times \bar{\mathbf{B}}}_{\text{Hall term}} - \underbrace{\frac{1}{en_e} \nabla p_e}_{\text{Electron pressure term}}$$

Faraday's law and electron pressure term:

$$\frac{\partial \bar{\mathbf{B}}}{\partial t} = -\nabla \times \bar{\mathbf{E}} = \frac{1}{e} \nabla \times \left(\frac{\nabla p_e}{n_e} \right)$$

$$\frac{\partial \bar{\mathbf{B}}}{\partial t} = \frac{1}{e} \nabla \times \left(\frac{\nabla(n_e k_B T_e)}{n_e} \right) = \frac{k_B}{e} \nabla \times \left(\frac{n_e \nabla T_e}{n_e} + T_e \frac{\nabla n_e}{n_e} \right) = \frac{k_B}{e} \left(\cancel{T_e \nabla \times \left(\frac{\nabla n_e}{n_e} \right)} + \nabla T_e \times \frac{\nabla n_e}{n_e} \right)$$

Consider an ideal gas: $p_e = n_e k_B T_e$

$$\frac{\partial \bar{\mathbf{B}}}{\partial t} = -\frac{k_B}{en_e} \nabla n_e \times \nabla T_e$$

Biermann battery
B-field generation

Turbulent dynamo



ARTICLE

DOI: [10.1038/s41467-018-02953-2](https://doi.org/10.1038/s41467-018-02953-2)

OPEN

Laboratory evidence of dynamo amplification of magnetic fields in a turbulent plasma

P. Tzeferacos^{1,2}, A. Rigby¹, A. F. A. Bott¹, A.R. Bell¹, R. Bingham^{3,4}, A. Casner⁵, F. Cattaneo², E.M. Churazov^{6,7}, J. Emig⁸, F. Fiuza⁹, C.B. Forest¹⁰, J. Foster¹¹, C. Graziani², J. Katz¹², M. Koenig¹³, C.-K. Li¹⁴, J. Meinecke¹, R. Petraso¹⁴, H.-S. Park⁸, B.A. Remington⁸, J.S. Ross⁸, D. Ryu¹⁵, D. Ryutov⁸, T.G. White¹, B. Reville¹⁶, F. Miniati¹⁷, A.A. Schekochihin¹, D.Q. Lamb², D.H. Froula¹² & G. Gregori^{1,2}

Abstract

Magnetic fields are ubiquitous in the Universe. The energy density of these fields is typically comparable to the energy density of the fluid motions of the plasma in which they are embedded, making magnetic fields essential players in the dynamics of the luminous matter. The standard theoretical model for the origin of these strong magnetic fields is through the amplification of tiny seed fields via turbulent dynamo to the level consistent with current observations. However, experimental demonstration of the turbulent dynamo mechanism has remained elusive, since it requires plasma conditions that are extremely hard to re-create in terrestrial laboratories. Here we demonstrate, using laser-produced colliding plasma flows, that turbulence is indeed capable of rapidly amplifying seed fields to near equipartition with the turbulent fluid motions. These results support the notion that turbulent dynamo is a viable mechanism responsible for the observed present-day magnetization.

<https://www.nature.com/articles/s41467-018-02953-2>

Turbulent dynamo

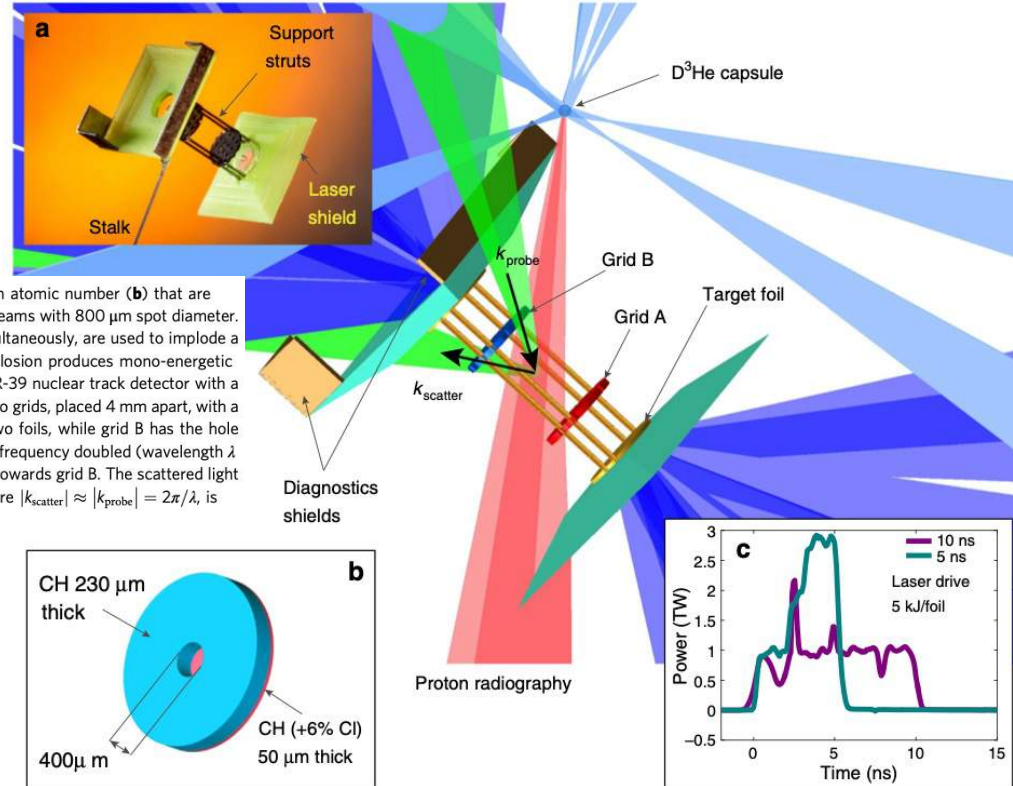


Fig. 1 Experimental configuration. The main target (see photo in **a**) consists of two CH foils doped with 6% chlorine in atomic number (**b**) that are separated by 8 mm. Each foil is illuminated by ten 500 J, 1 ns pulse length, frequency tripled (351 nm wavelength) laser beams with 800 μm spot diameter. The beams are stacked in time to achieve the two pulse profiles shown in **c**. An additional set of 17 beams, all fired simultaneously, are used to implode a 420 μm diameter capsule consisting of a 2- μm -thick SiO_2 shell filled with D_2 gas at 6 atm and ^3He at 12 atm. The implosion produces mono-energetic protons at 3.3 and 15 MeV with ~ 40 μm diameter source size, which traverse the plasma and are then collected by a CR-39 nuclear track detector with a total magnification factor of 28. The plasma expansion towards the center of the target is perturbed by the presence of two grids, placed 4 mm apart, with a 300 μm hole width and 300 μm hole spacing. Grid A has the central hole aligned on the center axis connecting the two foils, while grid B has the hole pattern shifted so that the central axis crosses the middle point between two holes. Thomson scattering uses a 30 J, 1 ns, frequency doubled (wavelength $\lambda = 526.5$ nm) laser beam to probe the plasma on the axis of the flow, 400 μm from the center and in a 50 μm focal spot, towards grid B. The scattered light is collected with 63° scattering angle and the geometry is such that the scattering wavenumber $k = k_{\text{scatter}} - k_{\text{probe}}$, where $|k_{\text{scatter}}| \approx |k_{\text{probe}}| = 2\pi/\lambda$, is parallel to the axis of the flow

Turbulent dynamo

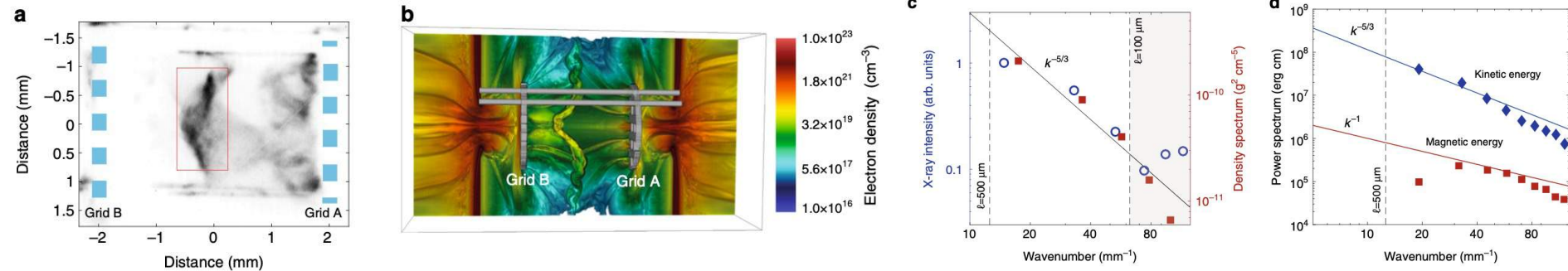
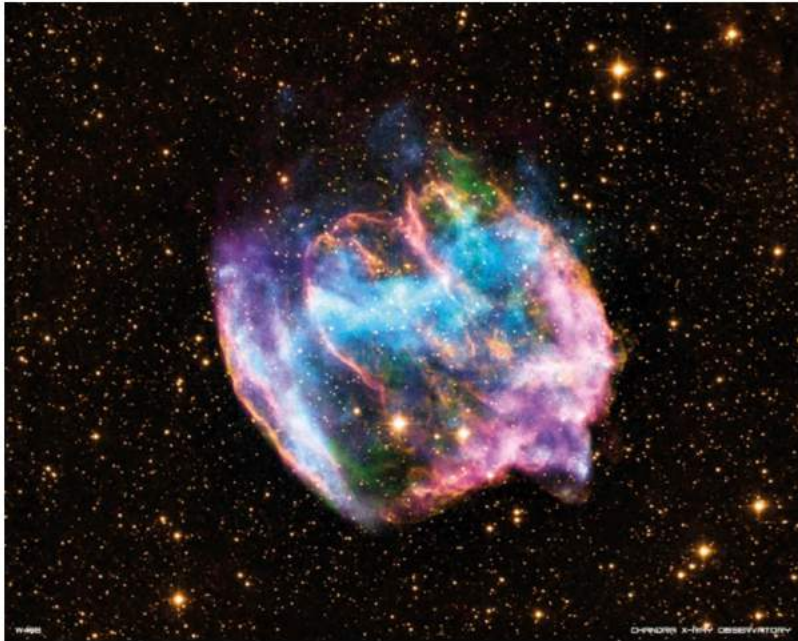


Fig. 2 Characterization of the plasma turbulence. **a** X-ray pinhole image of the colliding flows at $t = 35$ ns after the laser drive, using the 5 ns pulse profile. The image was recorded onto a framing camera with ~ 1 ns gate width and filtered with $0.5 \mu\text{m}$ C_2H_4 and $0.15 \mu\text{m}$ Al. The pinhole diameter is $50 \mu\text{m}$. **b** Rendering of the electron density from three-dimensional FLASH simulations at $t = 35$ ns. **c** The open blue circles give the power spectrum of the X-ray emission from the collision region, defined by the rectangular region shown in panel **a**. The power spectrum has been filtered to remove edge effects and image defects. Details of this procedure are given in Supplementary Methods. The shaded region at high wavenumbers is dominated by noise. The spectrum of the density fluctuations, as obtained from FLASH simulations in the turbulent region, is shown with red squares. **d** Blue diamonds: power spectrum of the kinetic energy from FLASH simulations. Red squares: power spectrum of magnetic energy from FLASH simulations. The simulated magnetic energy spectrum is considerably shallower than the Kolmogorov-like kinetic energy spectrum, as predicted by ref. ²³ and other studies in the $\text{Pm} < 1$ regime (see text)

Plasma instabilities: Weibel

Figure 1: Composite X-ray (blue and green), infrared (yellow and orange) and radio (pink) image of supernova remnant W49B, which is believed to be the result of a gamma-ray burst that took place a few thousand years ago in the Milky Way.



© X-ray: NASA/CXC/MIT/L.Lopez et al.; INFRARED: PALOMAR; RADIO: NSF/NRAO/VLA

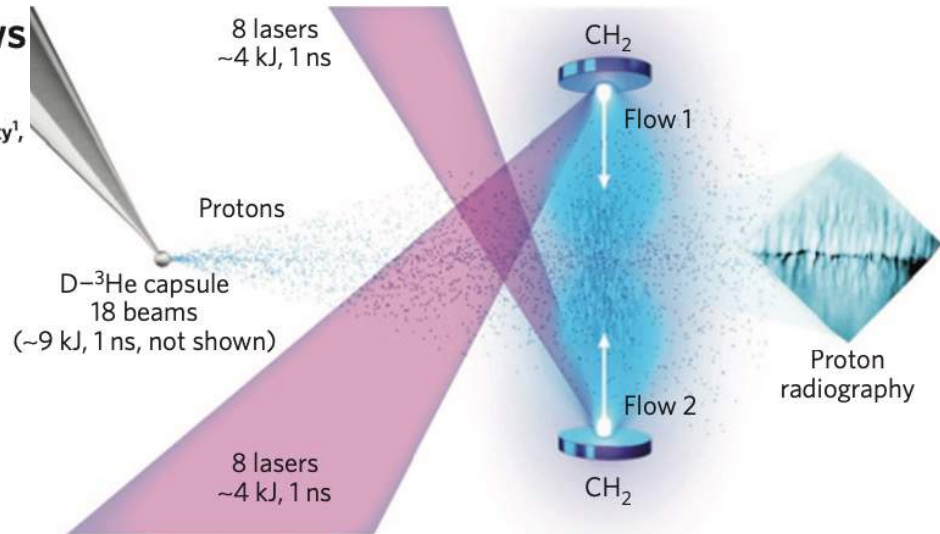
The Weibel instability is one candidate mechanism for the generation of sufficiently strong fields to create a collisionless shock.

Plasma instabilities: Weibel

Observation of magnetic field generation via the Weibel instability in interpenetrating plasma flows

C. M. Huntington^{1*}, F. Fiuza¹, J. S. Ross¹, A. B. Zylstra², R. P. Drake³, D. H. Froula⁴, G. Gregori⁵, N. L. Kugland⁶, C. C. Kuranz³, M. C. Levy¹, C. K. Li², J. Meinecke⁵, T. Morita⁷, R. Petrasso², C. Plechaty¹, B. A. Remington¹, D. D. Ryutov¹, Y. Sakawa⁷, A. Spitkovsky⁸, H. Takabe⁷ and H.-S. Park¹

Figure 1 | Experimental configuration to generate opposing plasma flows probed by D-³He protons. The experiment consists of a pair of (CH₂) plastic foils of diameter 2 mm and thickness 500 μm, oriented face-on and separated by 8 mm. Each was irradiated with eight overlapped laser beams, delivering ~4 kJ of 351 nm laser energy in a 1 ns square pulse. Distributed phase plates were used to produce super-Gaussian laser spots with focal spot diameters of 250 μm on the target surface. After a delay, the proton probe was created by laser-compressing a thin-walled SiO₂ capsule. The capsule was filled with a 1:1 mixture of deuterium (D) and ³helium (³He) at a total pressure of 18 atm. At peak compression (10²³ cm⁻³) protons are produced quasi-isotropically at energies of 3.0 and 14.7 MeV. The protons were detected using a CR39 nuclear track detector positioned on the midplane of the CH₂ target foils, such that the protons traverse the central interaction region as shown.



Plasma instabilities: Weibel

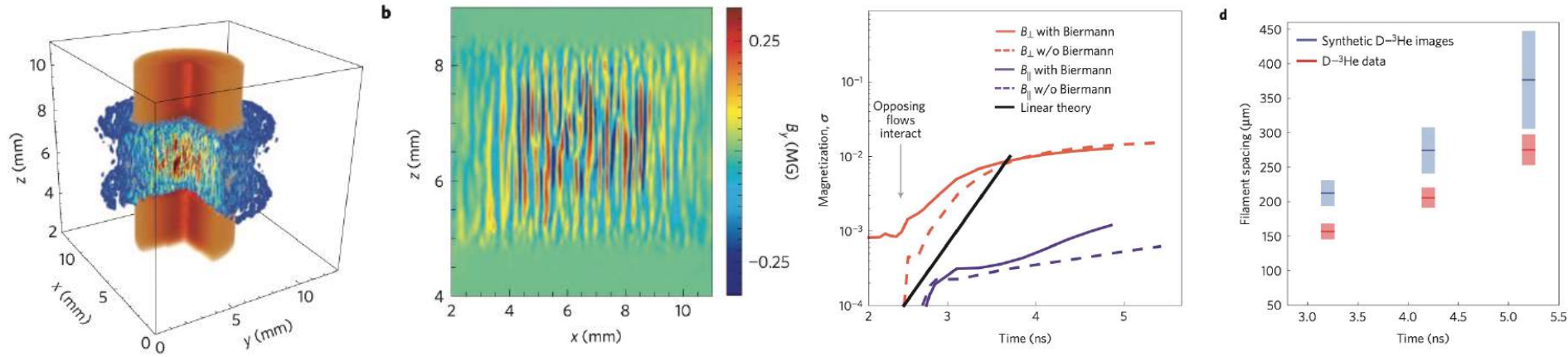
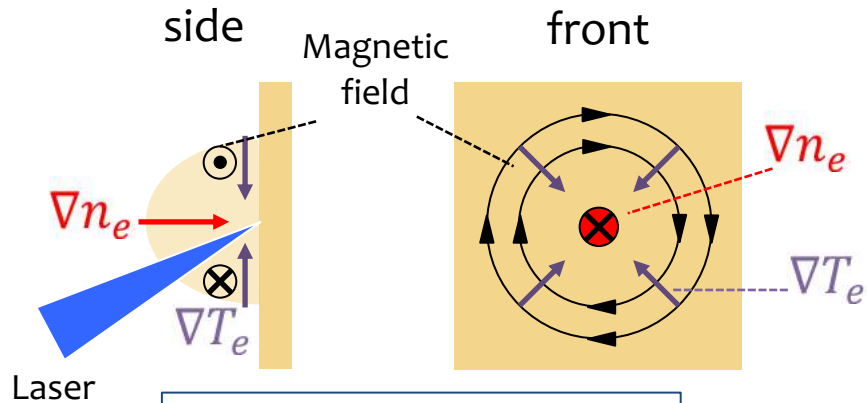


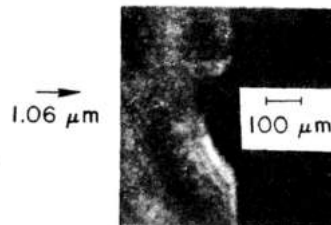
Figure 3 | Temporal evolution of magnetic field magnitude from simulation and field structure from experimental images. **a**, 3D OSIRIS simulation of the system after 1 ns of interaction between the counter-streaming $1,900 \text{ km s}^{-1}$ plasma flows (approximately 3 ns after the experimental drive laser pulse; flows enter from top and bottom). Magnetic fields are shown qualitatively in the blue/red colour scale, with electron density in orange. **b**, Magnetic field slice (transverse magnetic field component B_y) along the y -axis midplane, at the same time, illustrating the presence of strong filaments associated with the Weibel instability. **c**, Plasma magnetization, σ , as a function of time. When the flows are initiated with zero initial magnetic field (dashed lines) the magnetizations remain at zero until the flows begin interacting, between 2 and 3 ns. When initial toroidal fields are included consistent with the Biermann-battery mechanism, the perpendicular magnetization is $\sim 0.1\%$ before the flows interact (solid coloured lines). In both cases the magnetic energy associated with Weibel instability increases sharply after the flows interact, increasing σ by a factor greater than ten in several ns. The magnetization due to the ion Weibel instability, growing at the theoretical linear growth rate, is shown in solid black. This calculation shows that the Weibel-generated magnetization becomes the dominant contribution to the overall magnetization of the system. **d**, Measurement of the mean separation between filaments in experimental proton radiographs (red) and synthetic proton images from 3D PIC simulations (blue). The filament spacing approximately doubles over the 2 ns of observation. Note that time is experimental time, measured with respect to the beginning of the drive laser.

Laser-plasma generated magnetic fields

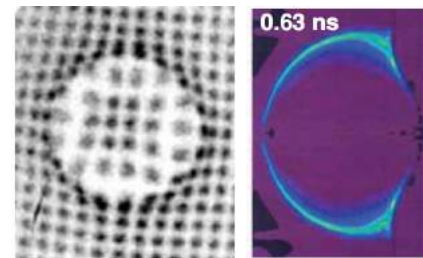
Nanosecond pulses, $I \sim 10^{14} \text{ Wcm}^{-2}$
 $B \sim 1 \text{ MG}$
 $v_B \sim 10^5 \text{ ms}^{-1}$



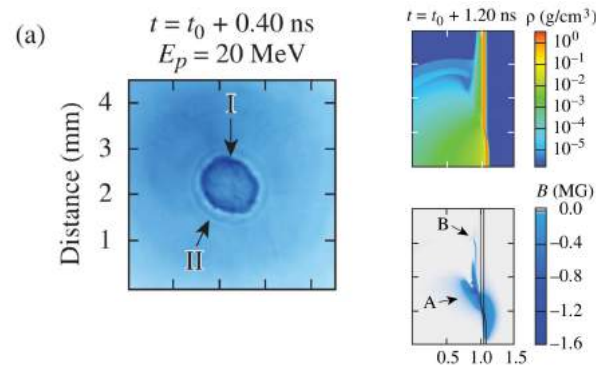
$$\frac{\partial \mathbf{B}}{\partial t} = \frac{k_B}{en_e} \nabla T_e \times \nabla n_e$$



$\Delta \phi = 16^\circ$
 JA Stamper and BH Ripen,
 PRL, 34, 138 (1975)

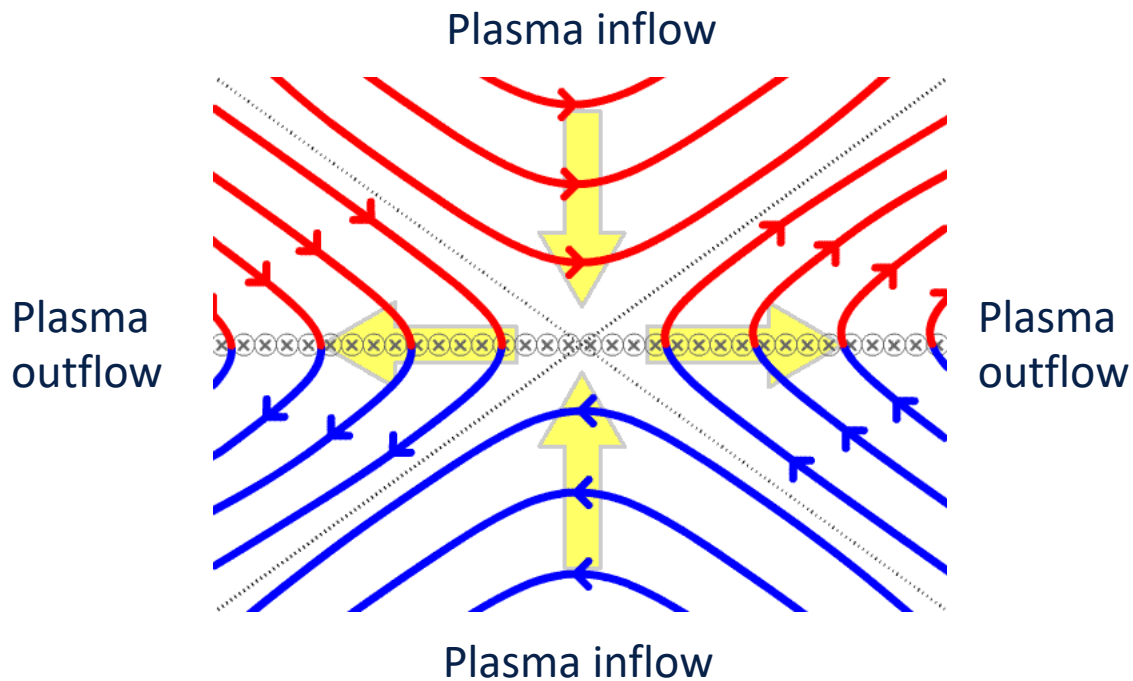


CK Li, et al., PRL, 97, 255001 (2006)



L. Gao et al. PRL, 114, 215003 (2015)

Magnetic reconnection

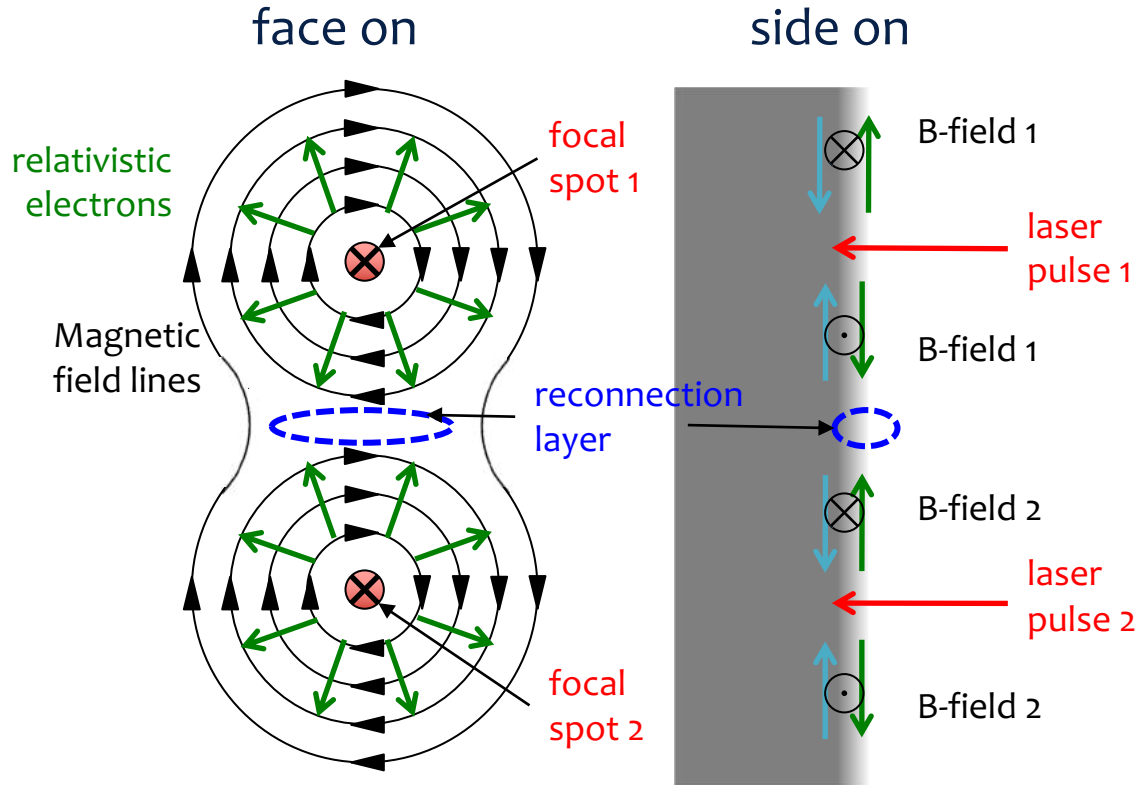


$$\text{Magnetic energy} = \frac{B^2}{2\mu_0}$$



Particle kinetic energy

Laser driven magnetic reconnection



Z-pinch driven magnetic reconnection

PRL 118, 085001 (2017)

PHYSICAL REVIEW LETTERS

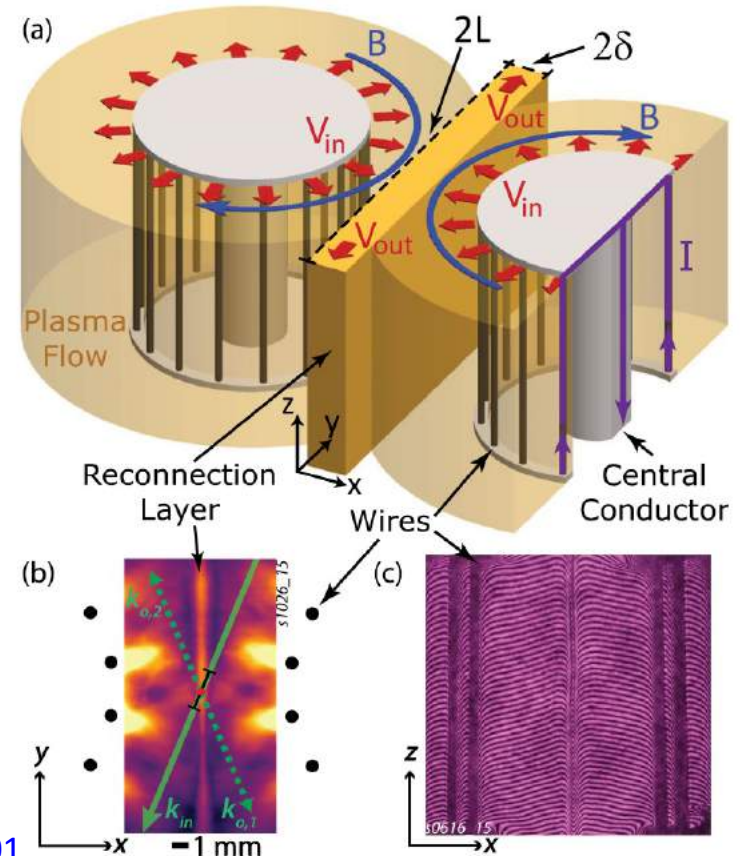
week ending
24 FEBRUARY 2017

Anomalous Heating and Plasmoid Formation in a Driven Magnetic Reconnection Experiment

J. D. Hare,^{1,*} L. Suttle,¹ S. V. Lebedev,^{1,†} N. F. Loureiro,² A. Ciardi,³ G. C. Burdiak,¹ J. P. Chittenden,¹ T. Clayson,¹ C. Garcia,¹ N. Niasse,¹ T. Robinson,¹ R. A. Smith,¹ N. Stuart,¹ F. Suzuki-Vidal,¹ G. F. Swadling,^{1,‡} J. Ma,⁴ J. Wu,⁵ and Q. Yang⁶

The colliding plasma flows were supersonic ($M_s \sim 1.6$) but sub-Alfvénic ($M_A \sim 0.7$), and therefore the thermal and dynamic plasma betas (ratio of the thermal or ram pressure to the magnetic pressure) are close to unity ($\beta_{th} \sim 0.7$, $\beta_{dyn} \sim 0.9$). These parameters are significantly different from those found both in magnetically driven experiments, such as MRX, and in laser driven experiments,

FIG. 1. (a) Experimental setup with the geometry of the reconnection layer. The cutaway on the right array shows the current path. (b) Top view with density map (taken at $t = 272$ ns after current start) and Thomson scattering vectors. (c) Side view interferogram.



Z-pinch driven magnetic reconnection

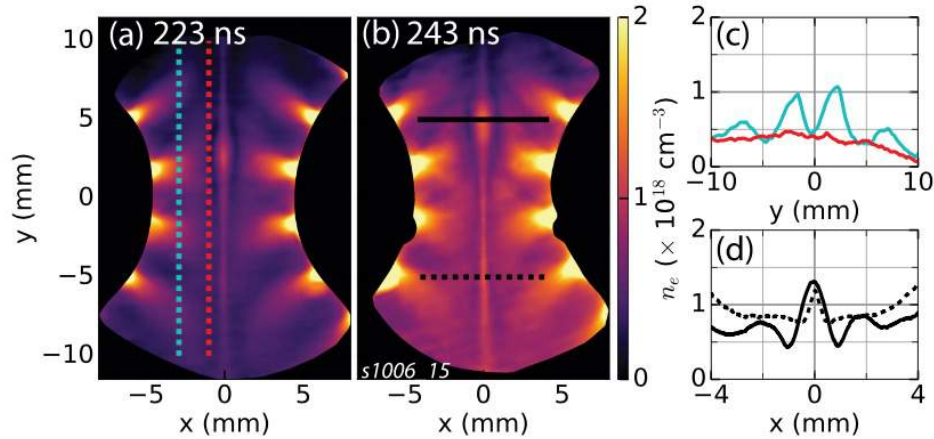


FIG. 2. Electron density maps from laser interferometry, both from the same shot. (a) At 223 ns after current start. (b) At 243 ns after current start. In both (a) and (b) there is an obvious region of enhanced density (a “plasmoid”) inside the reconnection layer. (c) Lineouts of electron density; x positions shown in (a). (d) Lineouts of electron density across the reconnection layer; y positions shown in (b).

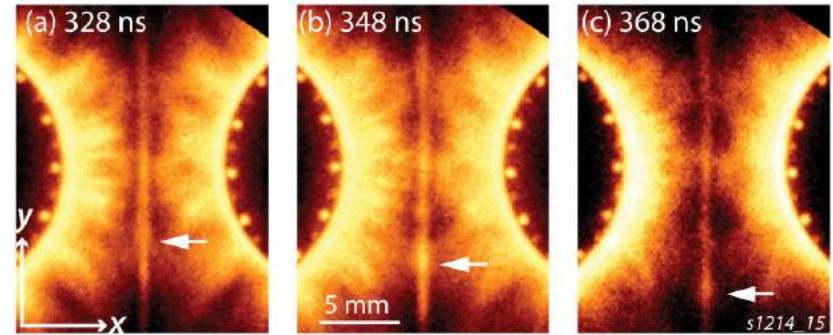
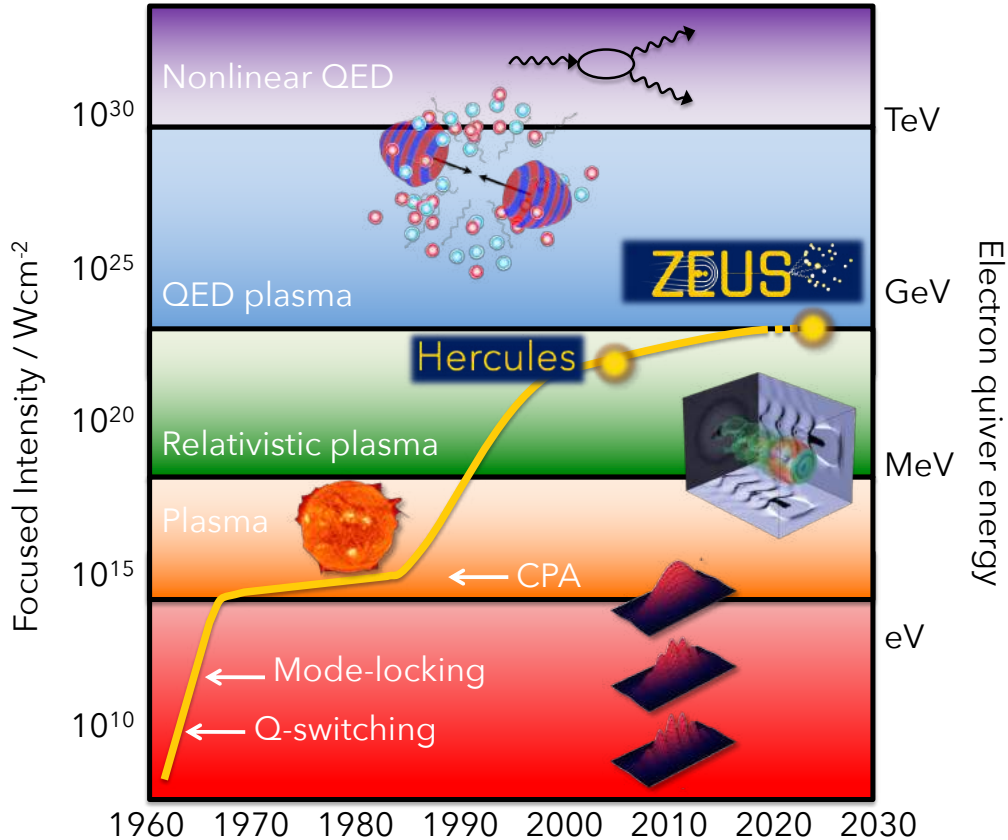


FIG. 5. Plasmoid formation and dynamics in three optical self-emission images from the same experiment: 5 ns exposure, 20 ns between frames. The location of one plasmoid in each frame is indicated with a white arrow.

Creating HEDP conditions: Laser pulses

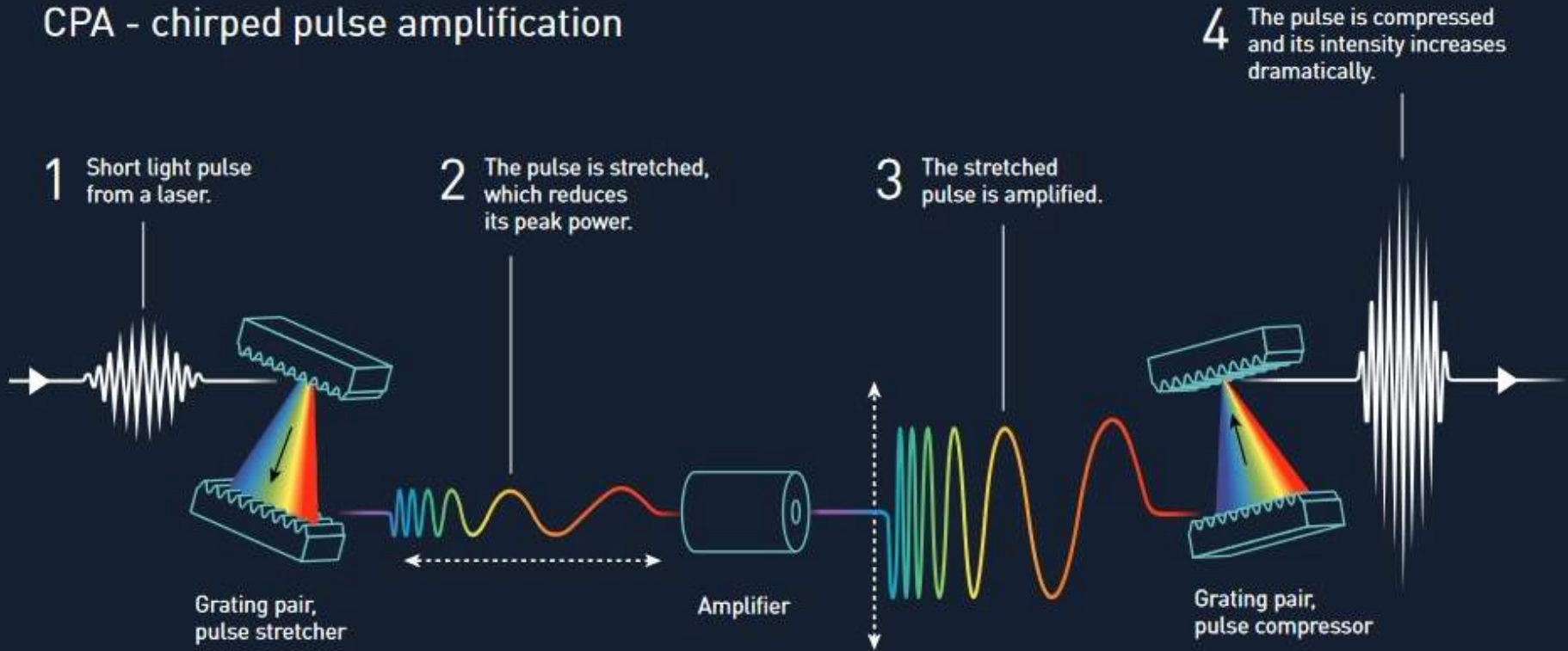


2018 Nobel prize for Physics awarded for CPA development



Chirped Pulse Amplification (CPA)

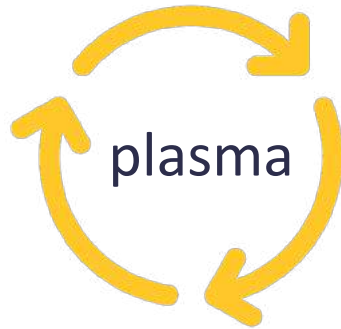
CPA - chirped pulse amplification



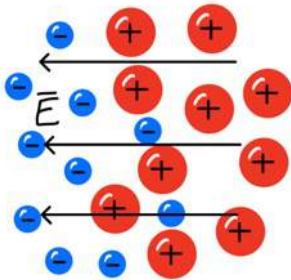
Laser Plasma Interactions



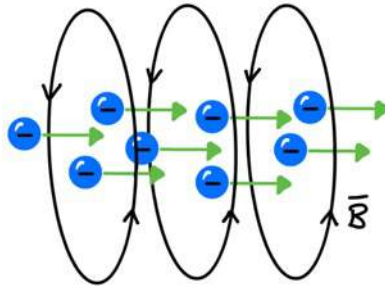
Electromagnetic fields
move charged particles



Generate
electric and
magnetic fields

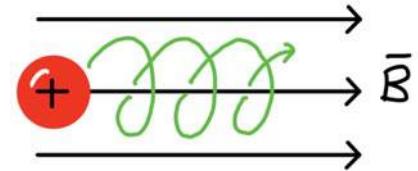
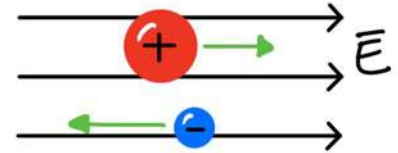


Currents
& charge
separation



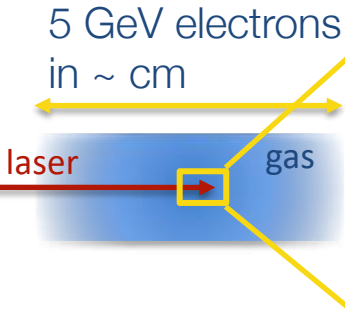
Force on a charged particle

$$F = \frac{dp}{dt} = q(\vec{E} + \vec{v} \times \vec{B})$$

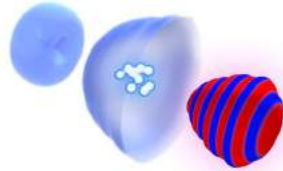


Laser Plasma Interactions

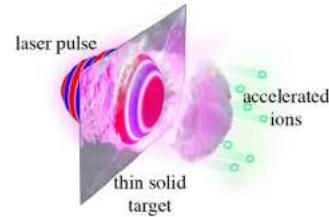
Plasma supports extremely strong field gradients for compact, unique, ultrashort duration particle and photon sources



Electron acceleration



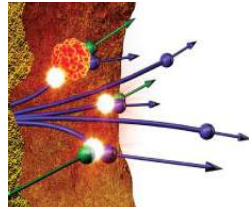
Ion acceleration



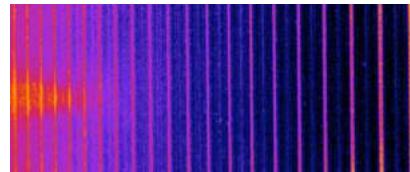
X-ray generation



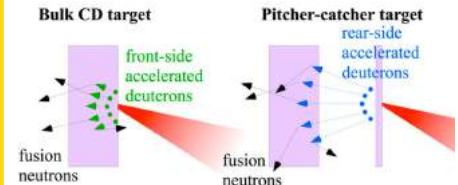
Positron production



High harmonic generation



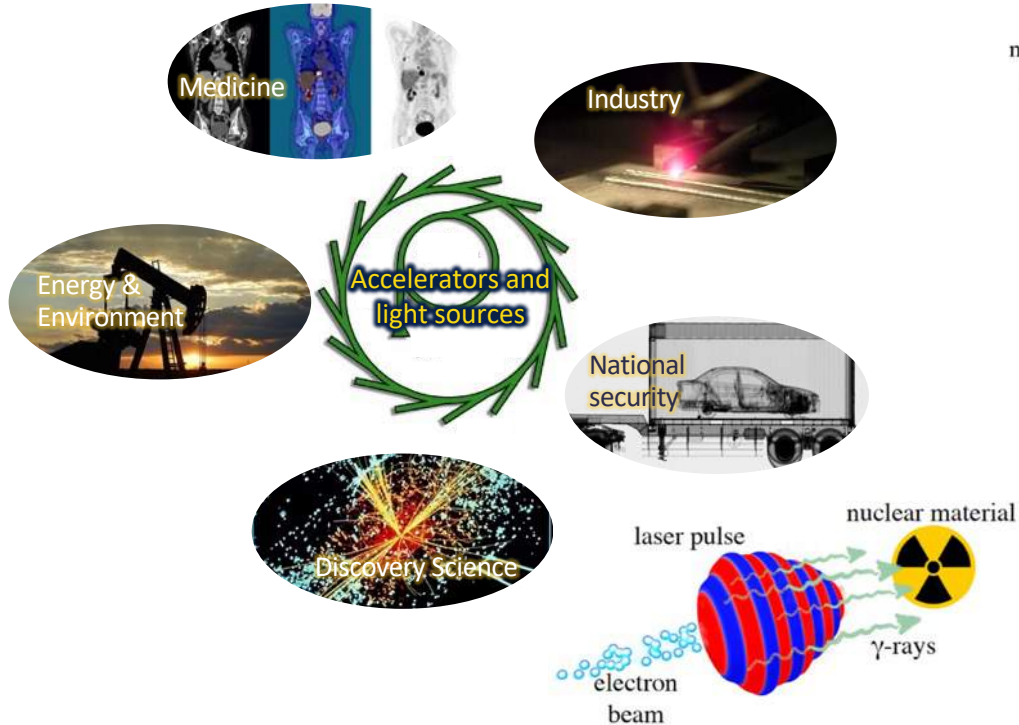
Neutron generation



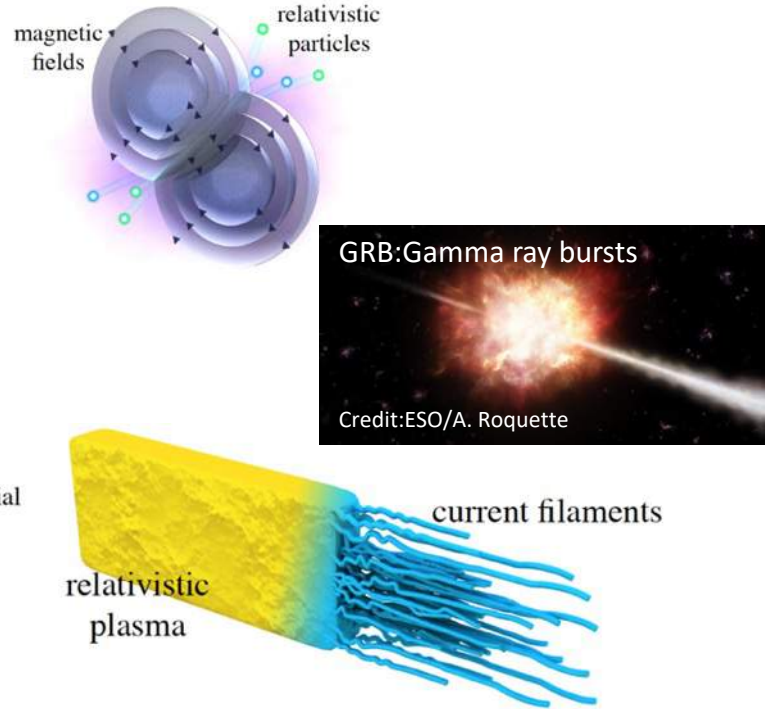
42 GeV electrons

Laser-driven source applications

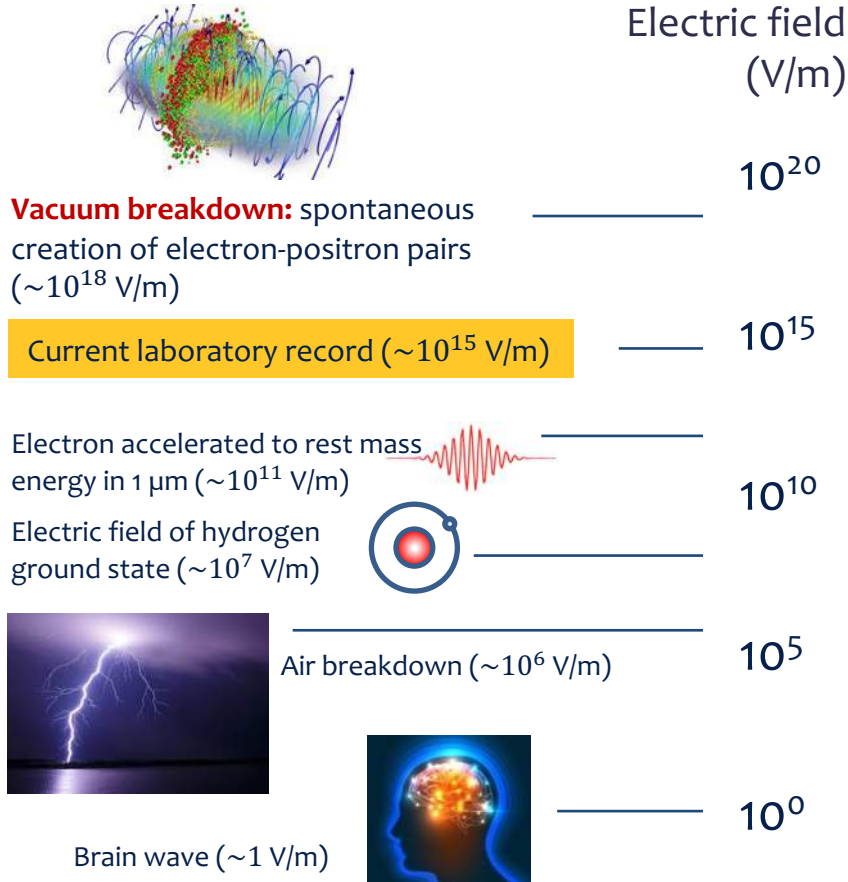
Particle and light source applications



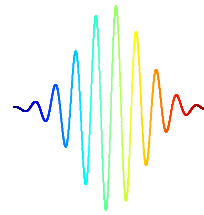
Probe for fundamental plasma processes



Laser Field Strength



Laser intensity:



$$I = \frac{\text{Energy}}{\text{Time} \times \text{Area}}$$

$$I = \frac{1}{2} \epsilon_0 c E^2$$

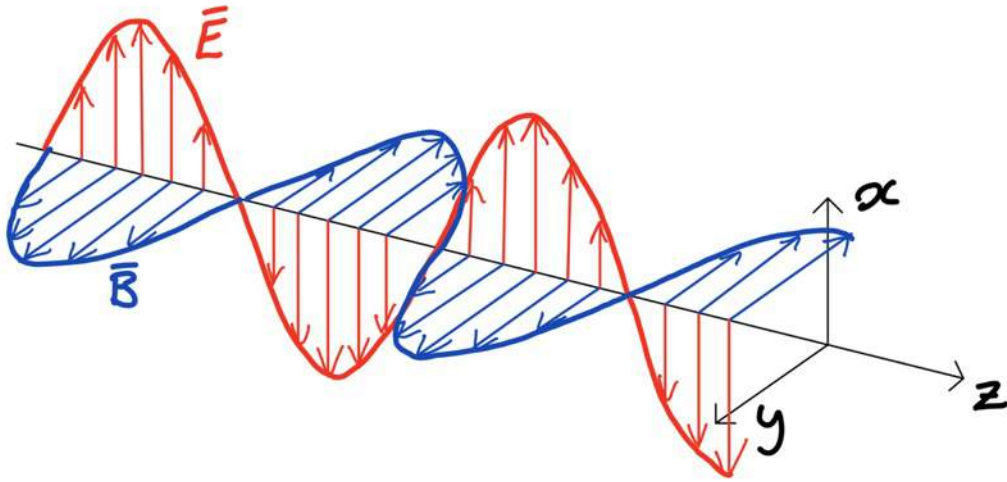
Lab record from a focused laser pulse*

$$I = 10^{23} \text{ W/cm}^2$$

$$\rightarrow E = 6 \times 10^{14} \text{ V/m}$$

*Record held by CoReLS; JW Yoon, et al., Optica, 8, 630 (2021)

What is high field science?



$$\bar{E} = \frac{\partial \bar{A}}{\partial t} = E_0 e^{-ikz} \hat{x}$$

$$\bar{B} = \nabla \times \bar{A} = B_0 e^{-ikz} \hat{y}$$

$$\bar{A} = \bar{A}_0 e^{-ikz}$$

Normalized vector potential

$$a = \frac{eA}{m_e c} = \frac{eE\lambda}{m_e c^2}$$

Relativistic regime, $a > 1$

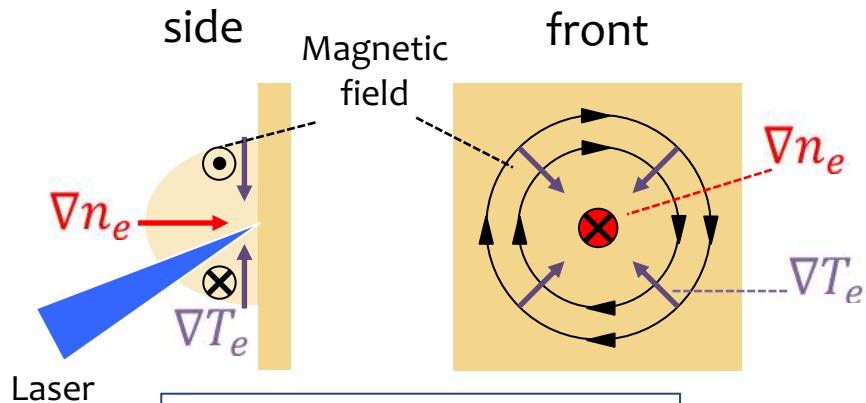
$$I = \frac{a_0^2}{\lambda_\mu^2 [\mu m]} 1.4 \times 10^{18} \text{ Wcm}^{-2}$$

Laser-plasma generated magnetic fields

Nanosecond pulses, $I \sim 10^{14} \text{ Wcm}^{-2}$

$B \sim 1 \text{ MG}$

$v_B \sim 10^5 \text{ ms}^{-1}$



$$\frac{\partial \mathbf{B}}{\partial t} = \frac{k_B}{en_e} \nabla T_e \times \nabla n_e$$

JA Stamper and BH Ripen, PRL, 34, 138 (1975);

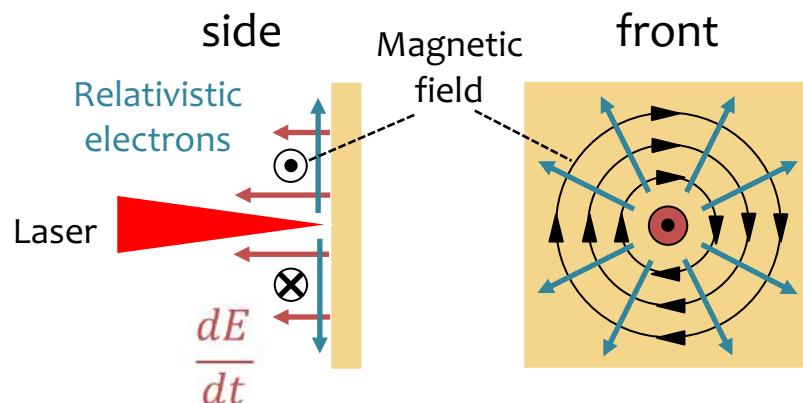
CK Li, et al., PRL, 97, 255001 (2006)

L. Gao et al. PRL, 114, 215003 (2015)

Picosecond pulses, $I \sim 10^{19} \text{ Wcm}^{-2}$

$B \sim 100 \text{ MG}$

$v_B \sim c$

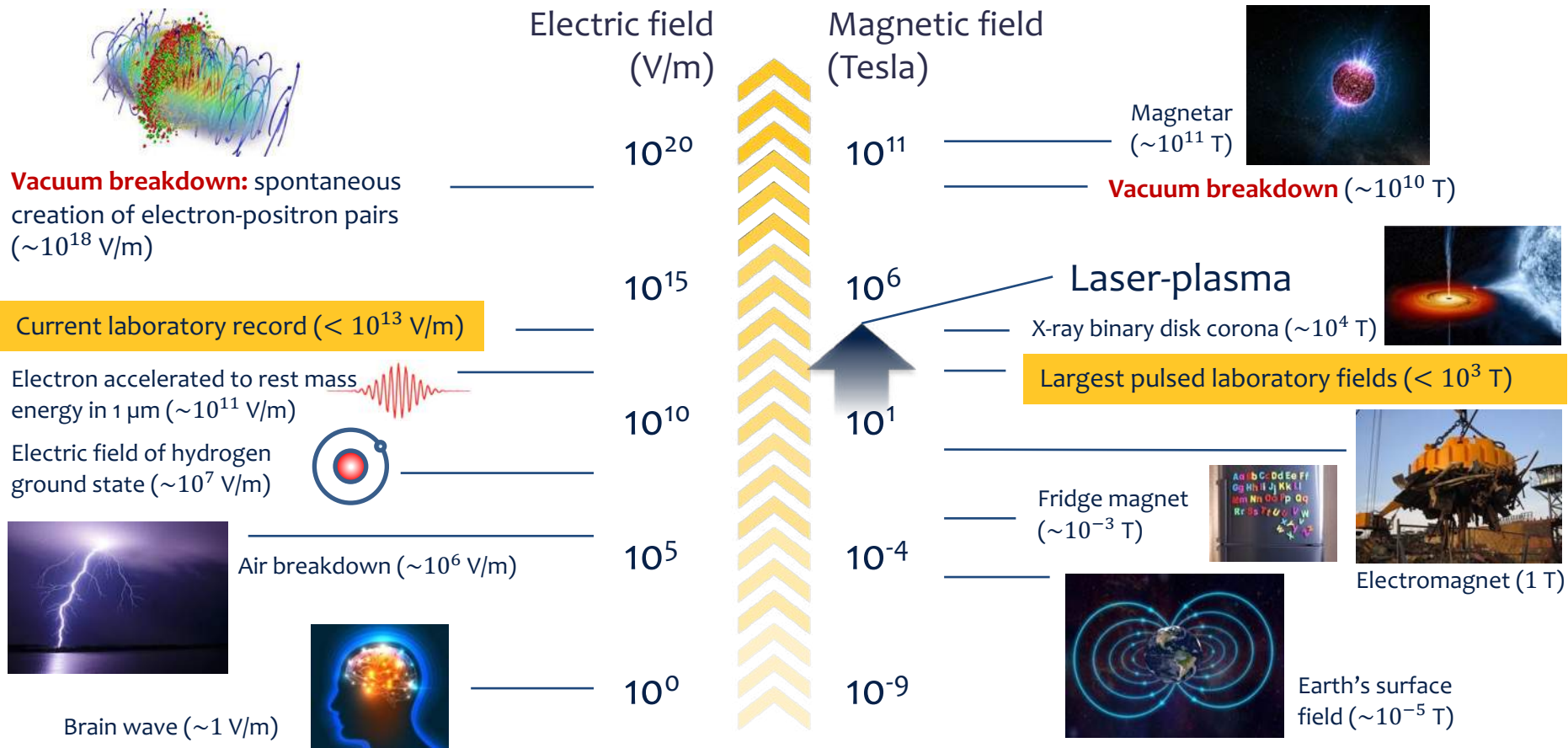


W. Schumaker et al. PRL, 110, 015003 (2013)

G. Sarri et al. PRL, 110, 255002 (2013)

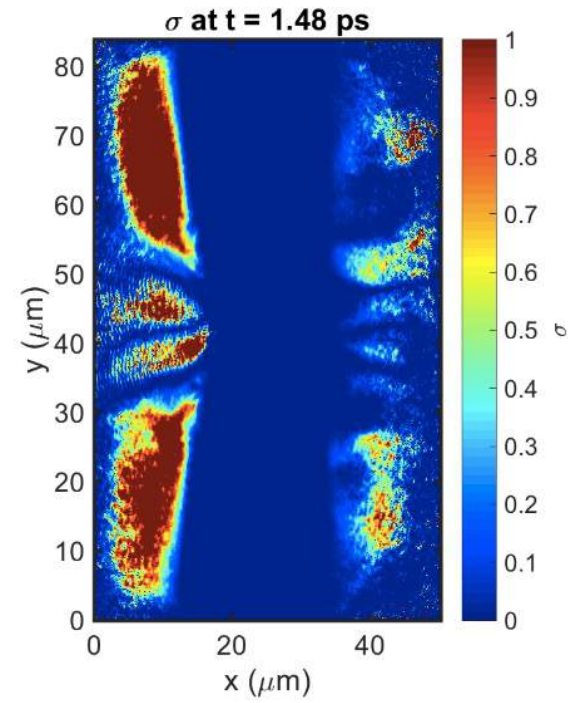
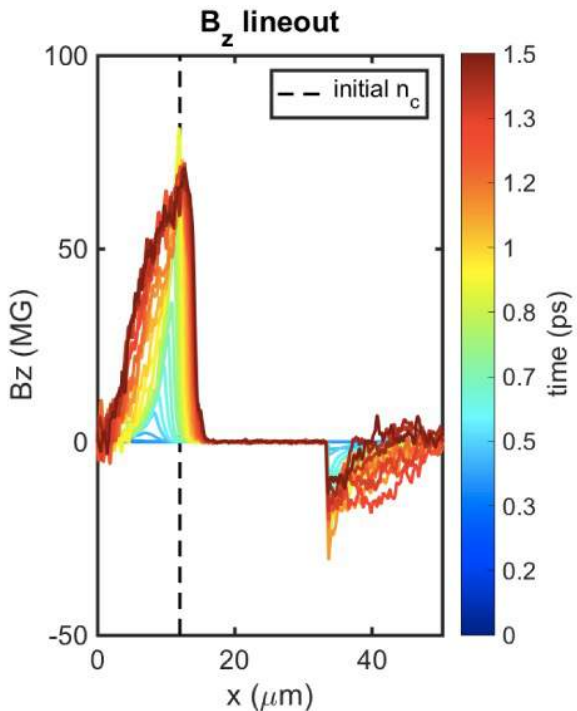
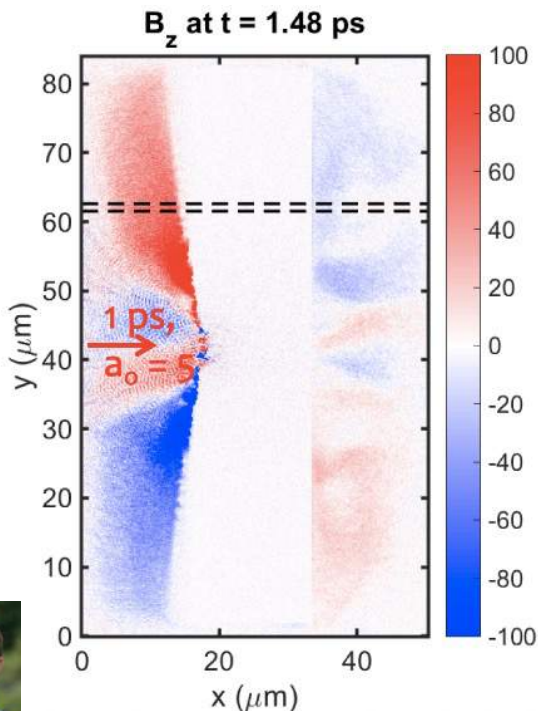
A. E. Raymond et al. PRE, 98, 043207 (2018)

Field Strength



Particle-in-cell simulations illustrate the magnetic field generation, dynamics and characteristics for picosecond interactions

$$\sigma_{cold} = \frac{B^2}{4\pi n_e m_e c^2}$$



OSIRIS Particle-in-cell simulation by Paul T Campbell

Simulations show the magnetic energy can exceed the rest mass energy to access a new regime in the laboratory

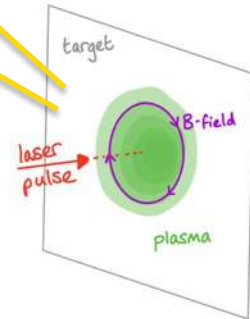
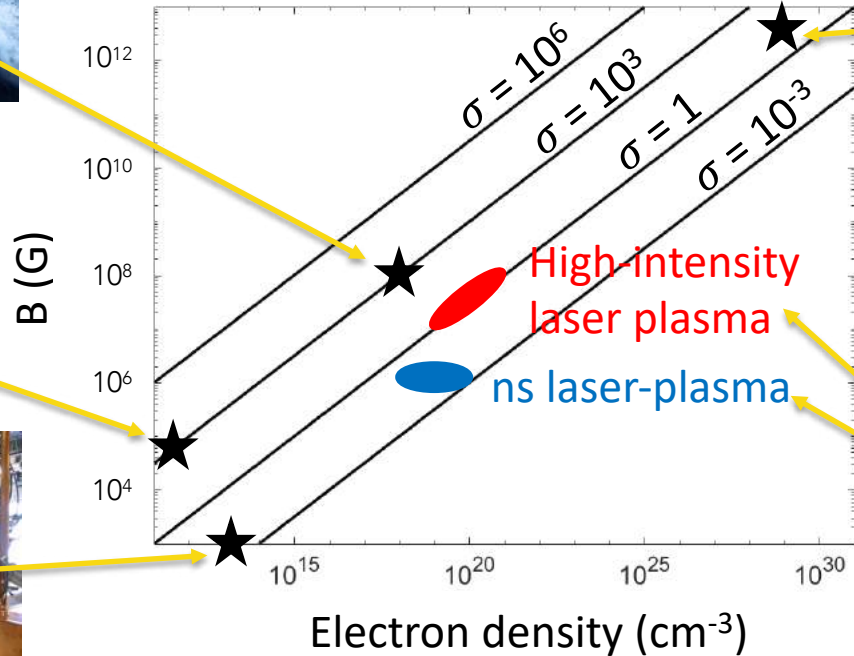


Credit: ESO/WFI (Optical); MPIfR/ESO/APEX/A.Weiss et al. (Submillimetre); NASA/CXC/CfA/R.Kraft et al. (X-ray)

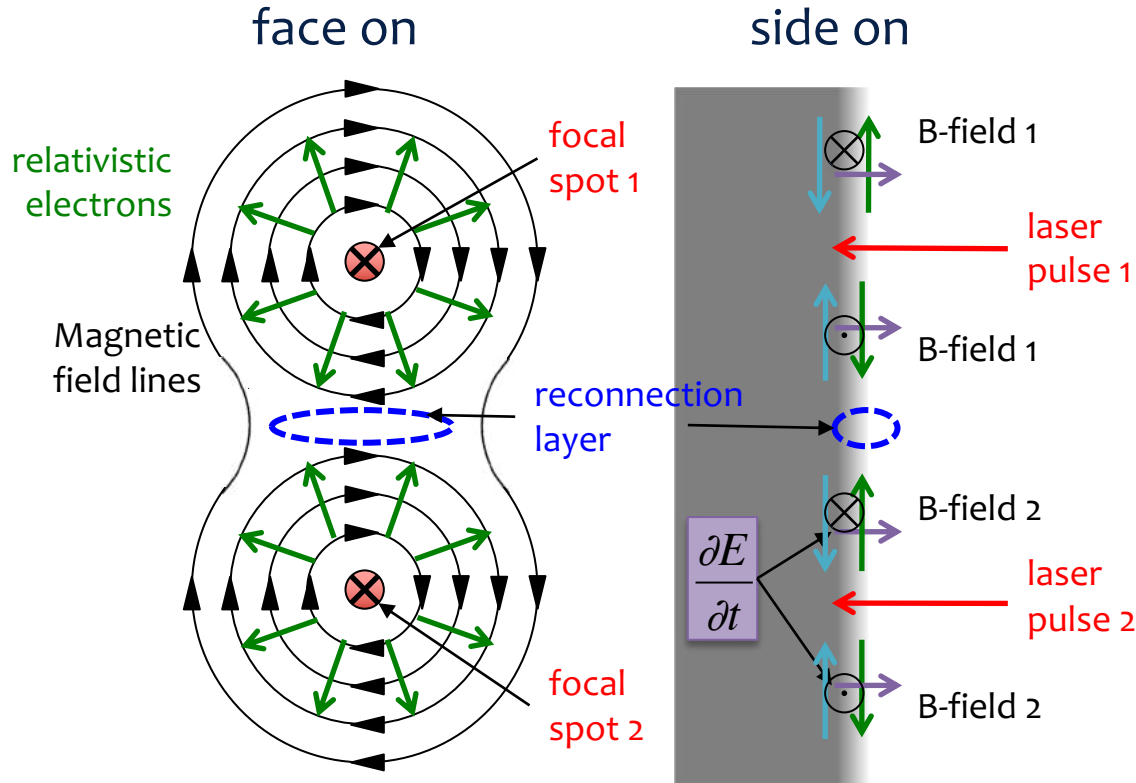


MRX: H Ji and W Daughton, et al., PoP (2011)

$$\sigma_{cold} = \frac{B^2}{4\pi n_e m_e c^2}$$

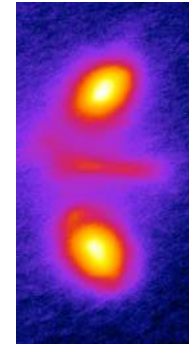


Relativistic electron driven magnetic reconnection is created by focusing 2 laser pulses in close proximity



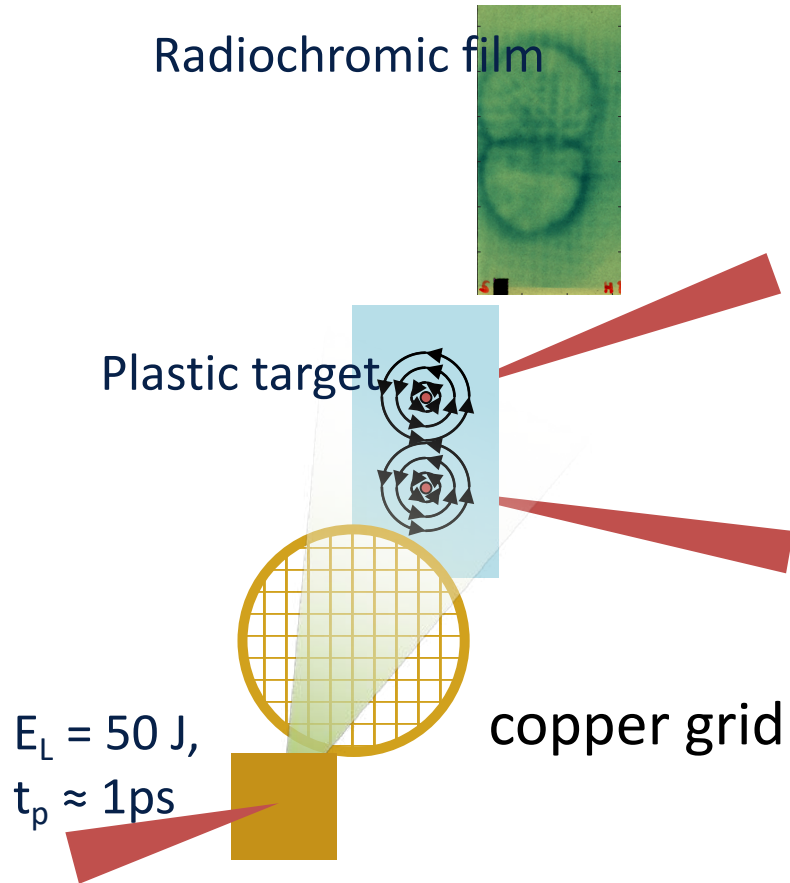
Magnetic field lines are driven together at $\sim c$

Surface layer has $\sigma_{cold} \geq 1$



Proton probing of a magnetic reconnection geometry at threshold relativistic intensity was performed at Vulcan (RAL)

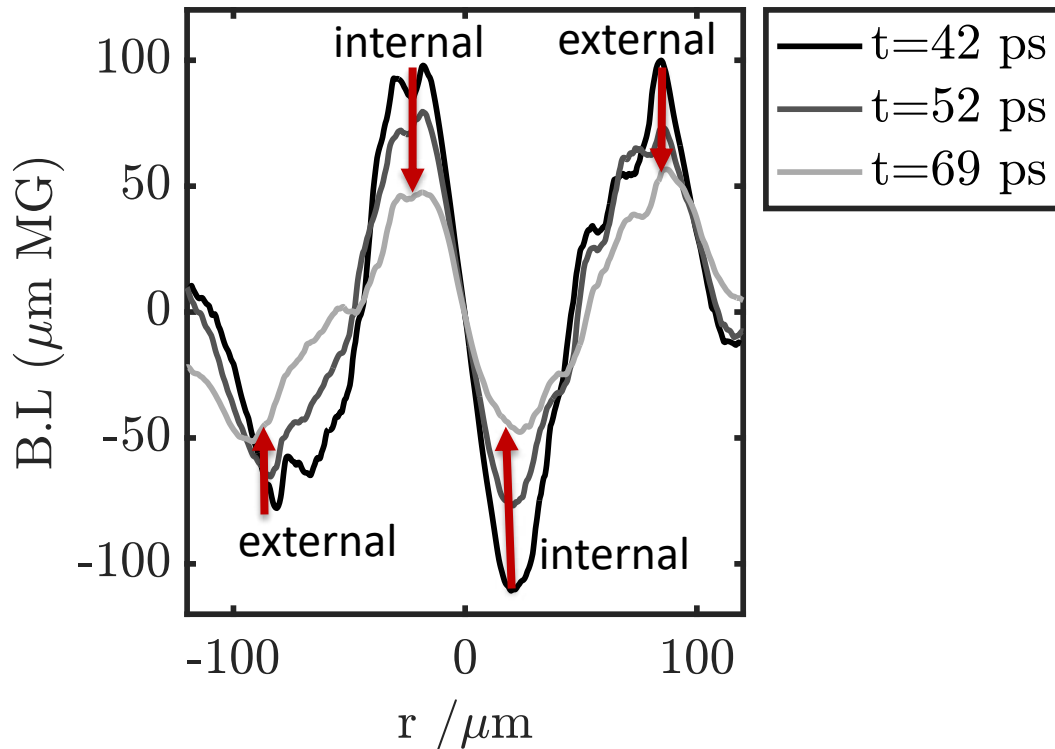
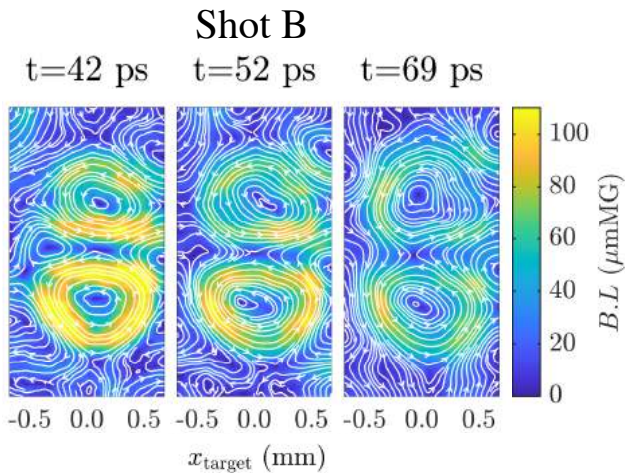
Charlotte Palmer



Vulcan Target Area West
Split mirror divides 100 J, 10 ps
 $I = 7 \times 10^{17} \text{ Wcm}^{-2}$ per focal spot

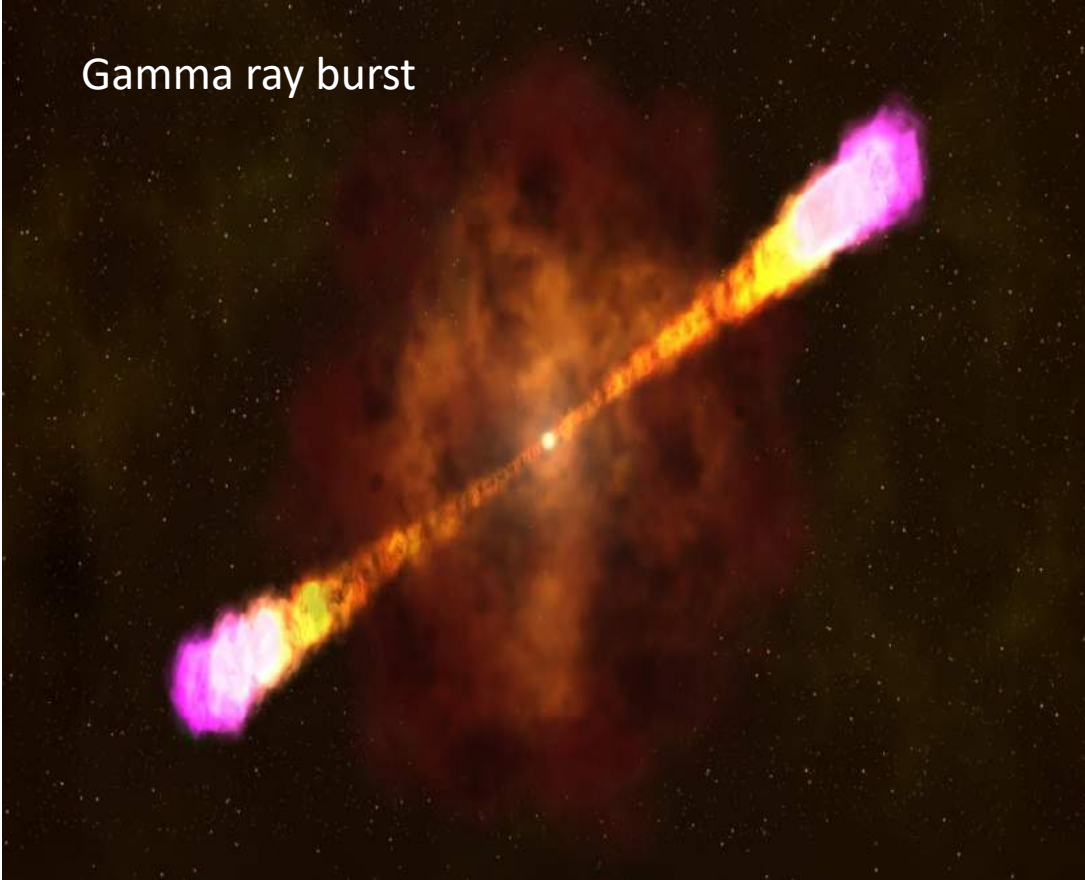
Proton probing of a magnetic reconnection geometry at close to threshold intensities was performed at Vulcan (RAL)

Field decays more rapidly internally than externally
→ could be due to magnetic reconnection

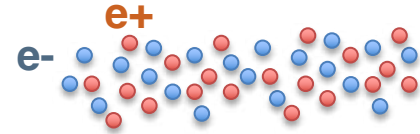


Can we create a pair plasma in the laboratory?

Gamma ray burst



Positrons have the same mass as electrons, but opposite charge.



The mass symmetry removes the separation of fast and slow scales present in electron-ion plasmas.

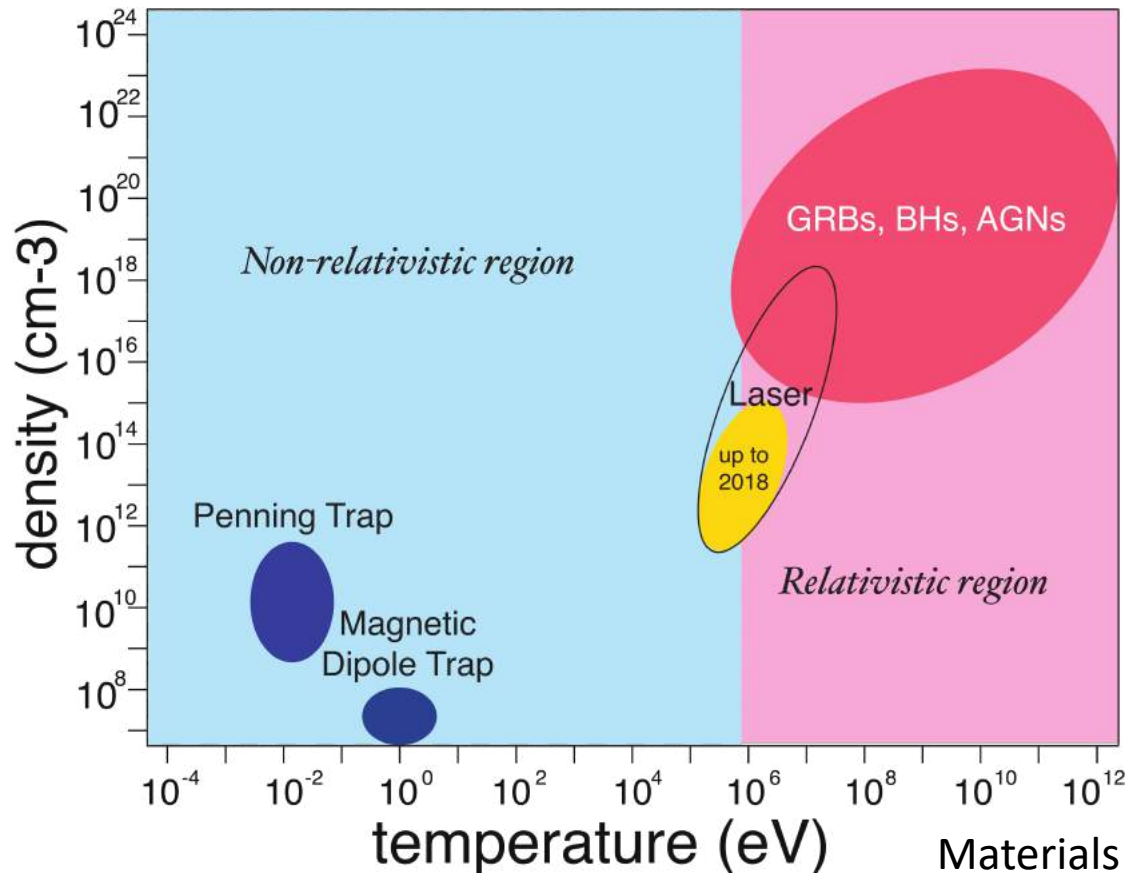
Tsyтович & Wharton (1978) Comments Plasma Phys. Controlled Fusion (1978)

Collisionless shocks of relativistic pair plasma could be drivers of gamma emission.

Liang et al. Scientific Reports (2015) Sarri et al. Nature (2015)

Materials from Hui Chen (LLNL)

Can we create a pair plasma in the laboratory?

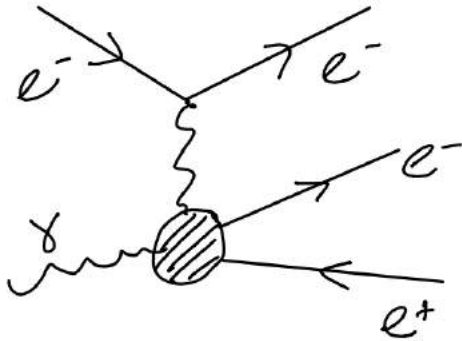


Materials from Hui Chen (LLNL)

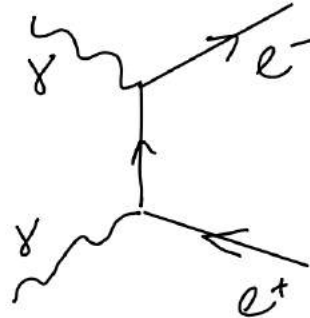
Can we create a pair plasma in the laboratory?

Positron generation processes

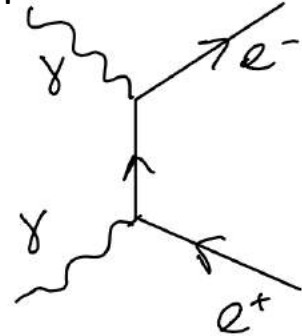
Trident process



Bethe-Heitler (BH) process



Breit-Wheeler process



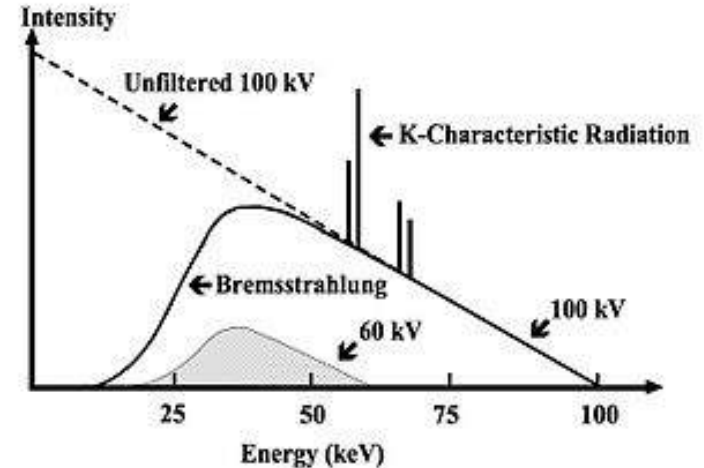
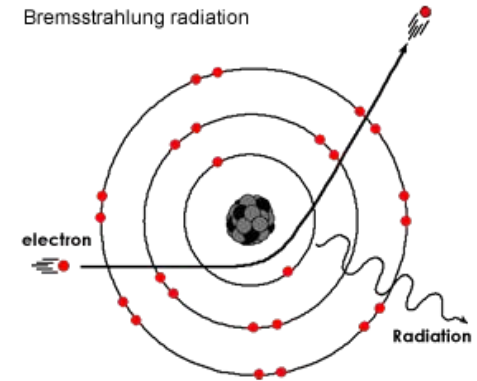
Need high energy electrons and photons

→ Generate high-energy photons through Bremsstrahlung

Can we create a pair plasma in the laboratory?

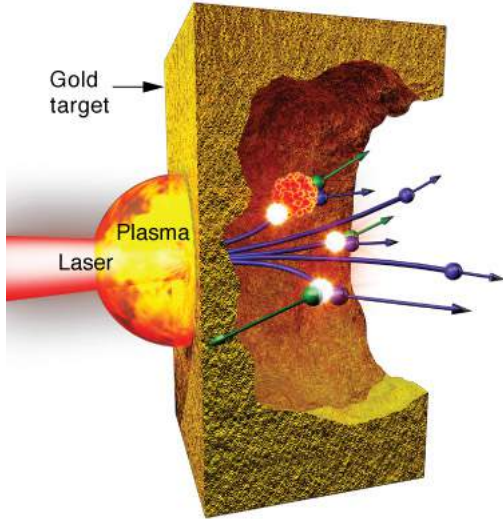
Bremsstrahlung (braking) radiation:

- Strong electric field of the atomic nuclei slows down and deflects an electron
- High Z nuclei have strongest effect
- Photon energies up to the highest energy electrons

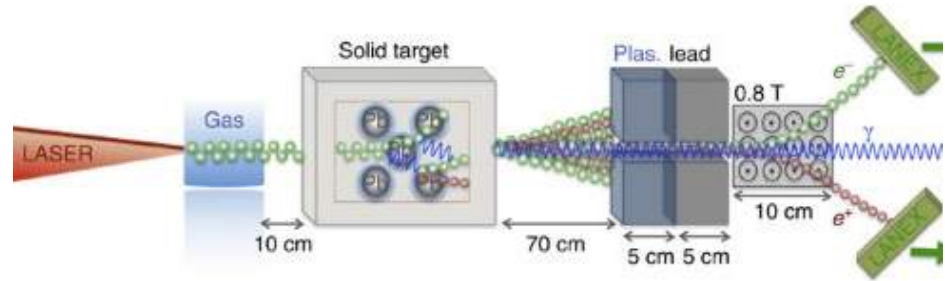


Can we create a pair plasma in the laboratory?

Laser plasma interactions can generate dense, relativistic energy electron beams



H Chen, et al., PRL, 102, 105001 (2009)



G Sarri, et al., PRL, 110, 255002 (2013)

Can we create a pair plasma in the laboratory?

PRL 114, 215001 (2015)

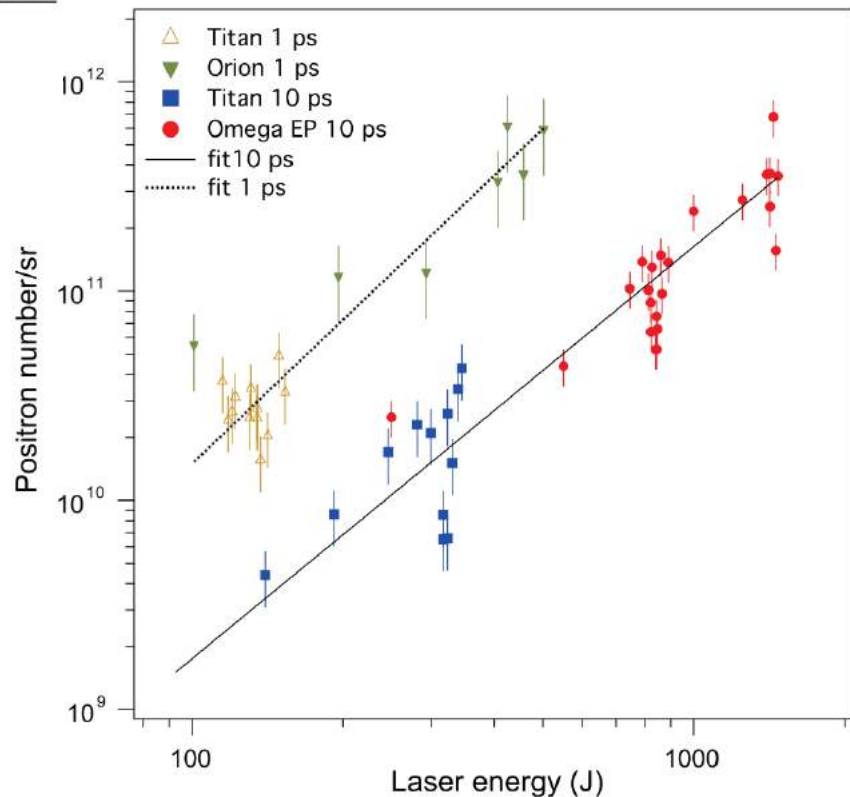
PHYSICAL REVIEW LETTERS

week ending
29 MAY 2015

Scaling the Yield of Laser-Driven Electron-Positron Jets to Laboratory Astrophysical Applications

Hui Chen,¹ F. Fiuza,^{1,2} A. Link,¹ A. Hazi,¹ M. Hill,³ D. Hoarty,³ S. James,³ S. Kerr,⁴ D. D. Meyerhofer,⁵ J. Myatt,⁵ J. Park,¹ Y. Sentoku,⁶ and G. J. Williams¹

FIG. 1 (color online). Dependence of the measured positron yield on the laser energy, E_L , obtained at three different laser facilities: Omega EP, Orion, and Titan. The upper group is from shots with 1 ps laser pulse: (brown) triangles Titan and (green) diamonds Orion. The lower group is obtained with 10 ps laser pulse: (blue) squares Titan and (red) circles Omega EP.



Can we create a pair plasma in the laboratory?

Requirements to achieve a pair plasma

- Debye length < system size

$$\lambda_D = \sqrt{\frac{\epsilon_0 k_B T_e}{e^2 n_e}}$$

Need $\left\{ \begin{array}{l} \text{large } n_e \\ \text{small } k_B T_e \end{array} \right.$ to keep system size modest

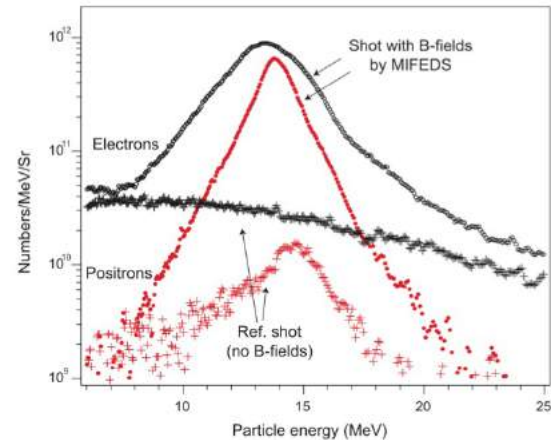
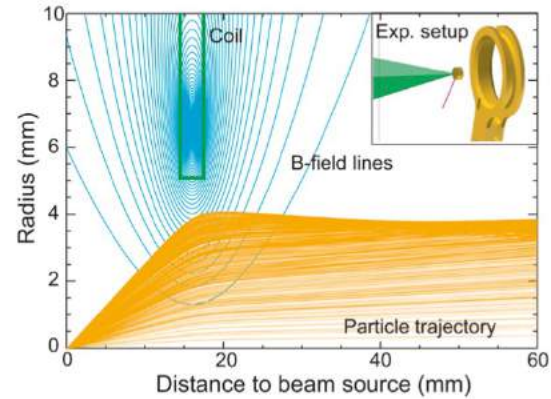
- System assembled for timescales > process of interest timescale

→ Need to confine the pairs → use a magnetic mirror?

Can we create a pair plasma in the laboratory?

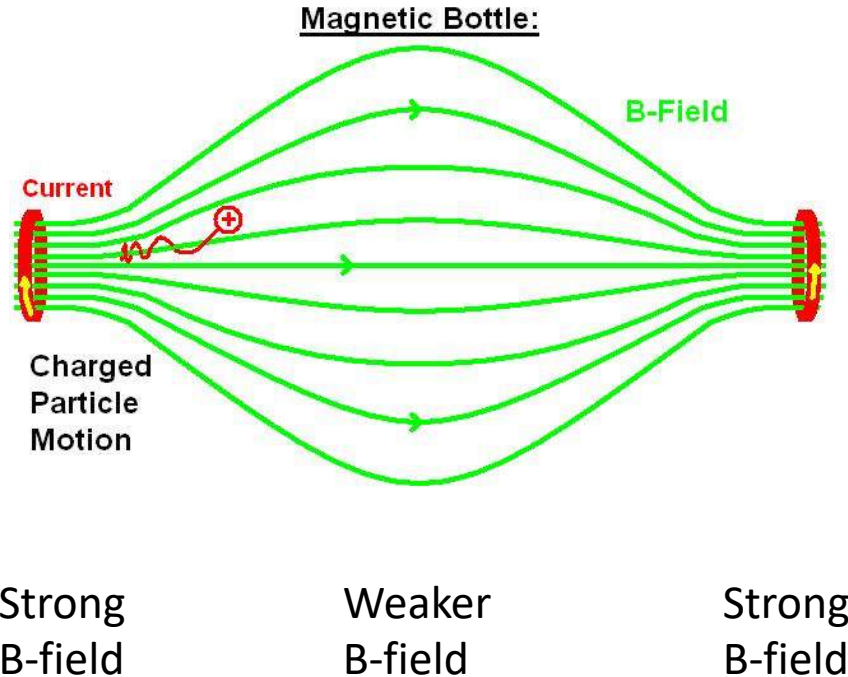
A magnetic pulse power coil focuses the positron beam

This creates an approaching quasi-neutral jet of pairs



Can we create a pair plasma in the laboratory?

Magnetic mirror



Assume particle's magnetic moment and total energy don't change \rightarrow magnetic moment:

$$\mu = \frac{mv_{\perp}^2}{2B}$$

In regions of larger B , v_{\perp} increases
But the total energy must remain constant:

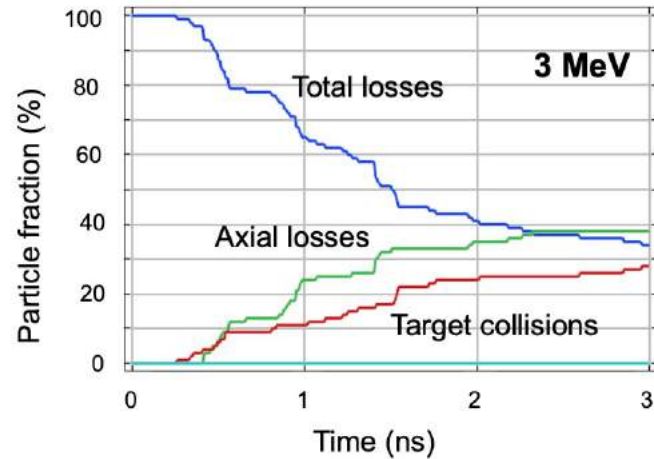
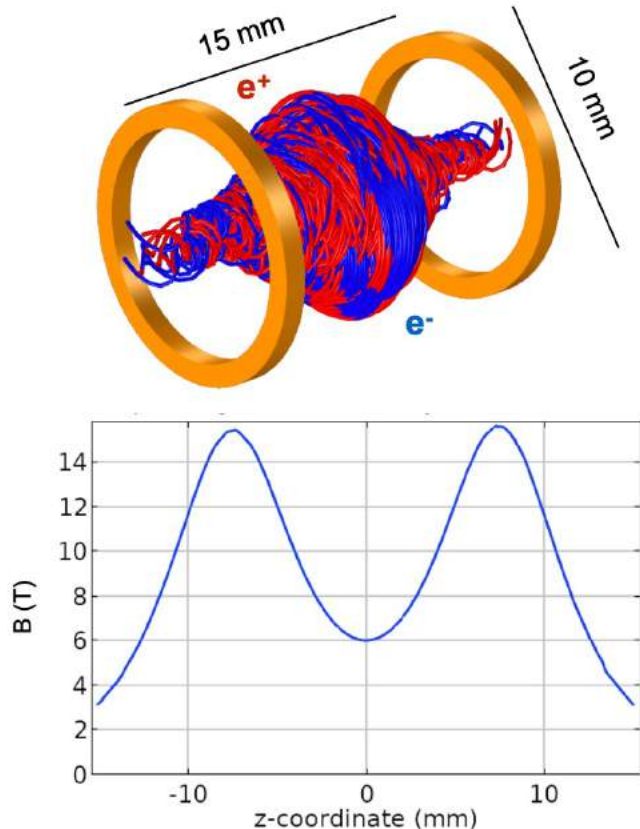
$$\varepsilon = q\phi + \frac{1}{2}mv_{\parallel}^2 + \frac{1}{2}mv_{\perp}^2$$

For $\phi = 0$, this means v_{\parallel} must drop, even go negative.

Particles bounce between coils.

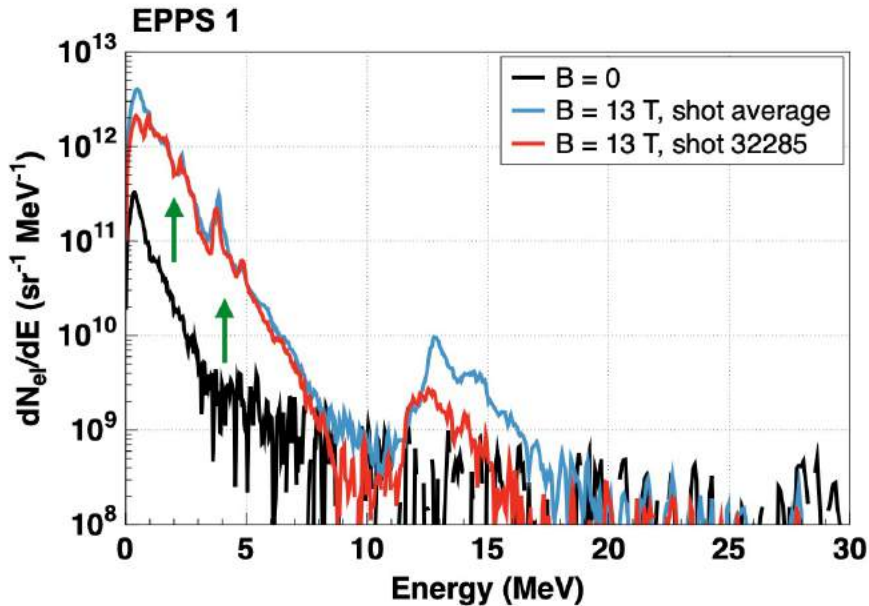
Can we create a pair plasma in the laboratory?

Particle tracking indicates good mirror confinement of < 3 MeV particles



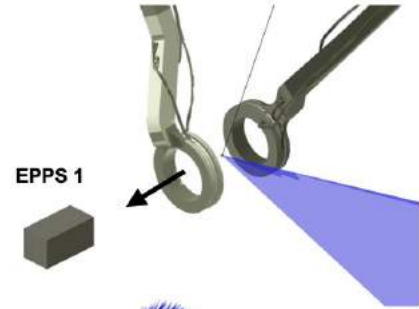
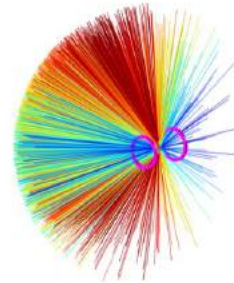
Can we create a pair plasma in the laboratory?

Axial losses increase with magnetic fields on



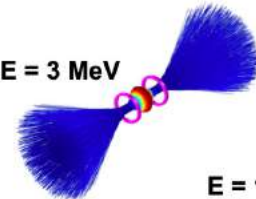
$E < 3 \text{ MeV}$ are well confined and only are lost axially
Axial flux of $3 \text{ MeV} < E < 15 < \text{MeV}$ is increased
15 MeV particles are focused by B-field

$B = 0$ All energies

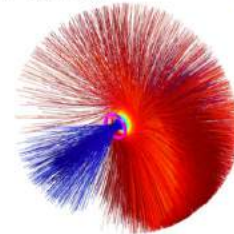


$B = 13 \text{ T}$

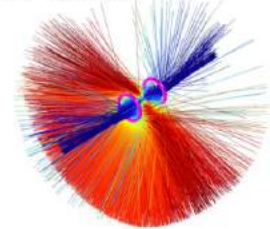
$E = 3 \text{ MeV}$



$E = 5 \text{ MeV}$



$E = 15 \text{ MeV}$



Can we create a pair plasma in the laboratory?

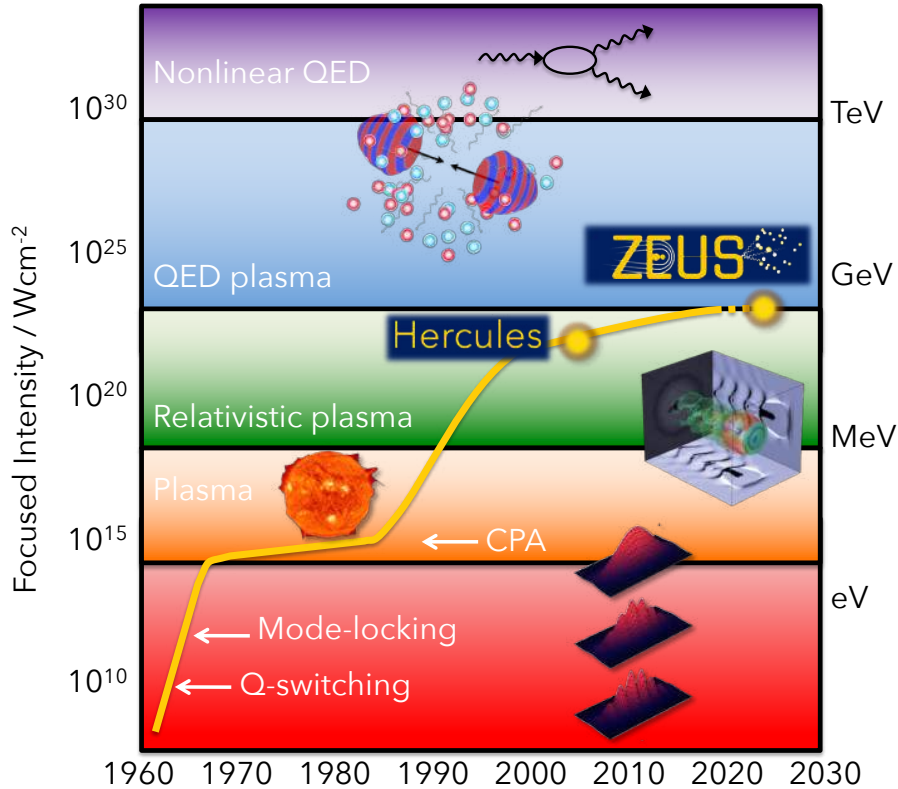
Highest positron yield = 10^{12} positrons

This 13 T magnetic mirror can contain a pairs for times of \sim nanoseconds, with $\gamma \approx 6$ and magnetization $\sigma \approx 40$. The Debye length and skin depth approach unity.

To achieve more significant pair plasma, need:

- To increase positron yield and decrease the average energy of the positrons
- And/or increase the magnetic field (to increase the particle energy that can be trapped)

Laser Intensity Frontier



TeV $\rightarrow \chi = 1$
(lepton at rest)

GeV $\rightarrow \chi = 1$
(lepton at energy $\sim a_0 m_e c^2$)

MeV $\rightarrow a_0 = 1$

Electron quiver energy

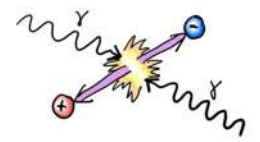
Quantum nonlinearity parameters:

$$\chi_e = \frac{\|F_{\mu\nu} v^\nu\|}{E_{cr}} = \frac{\text{Amplitude of } E \text{ in } e \text{ rest frame}}{E_{cr}}$$

$$\chi_\gamma = \frac{\|F_{\mu\nu} \hbar k^\nu\|}{m_e E_{cr}} = \frac{\text{Amplitude of } E \text{ in } e^+e^- \text{ center of mass}}{E_{cr}}$$

Classical nonlinearity parameter:

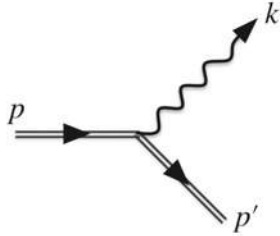
$$a = \frac{1}{2\pi} \frac{eE\lambda}{m_e c^2} = \frac{\text{Quiver energy of electron}}{m_e c^2}$$



Laser Intensity Frontier

Nonlinear Compton emission:

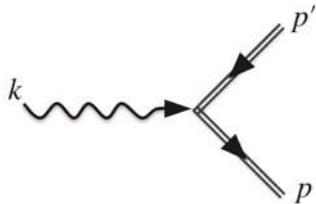
Photon emission by a (dressed) electron



Modifies charged
particle dynamics

Multi-photon Breit-Wheeler

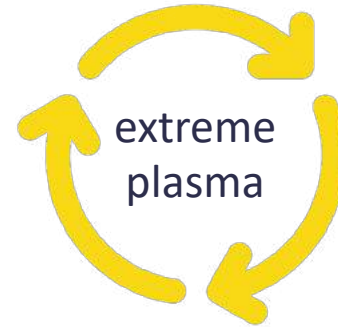
Decay of a photon to a (dressed) pair



Modifies charged
particle density

EM-fields move
charged particles

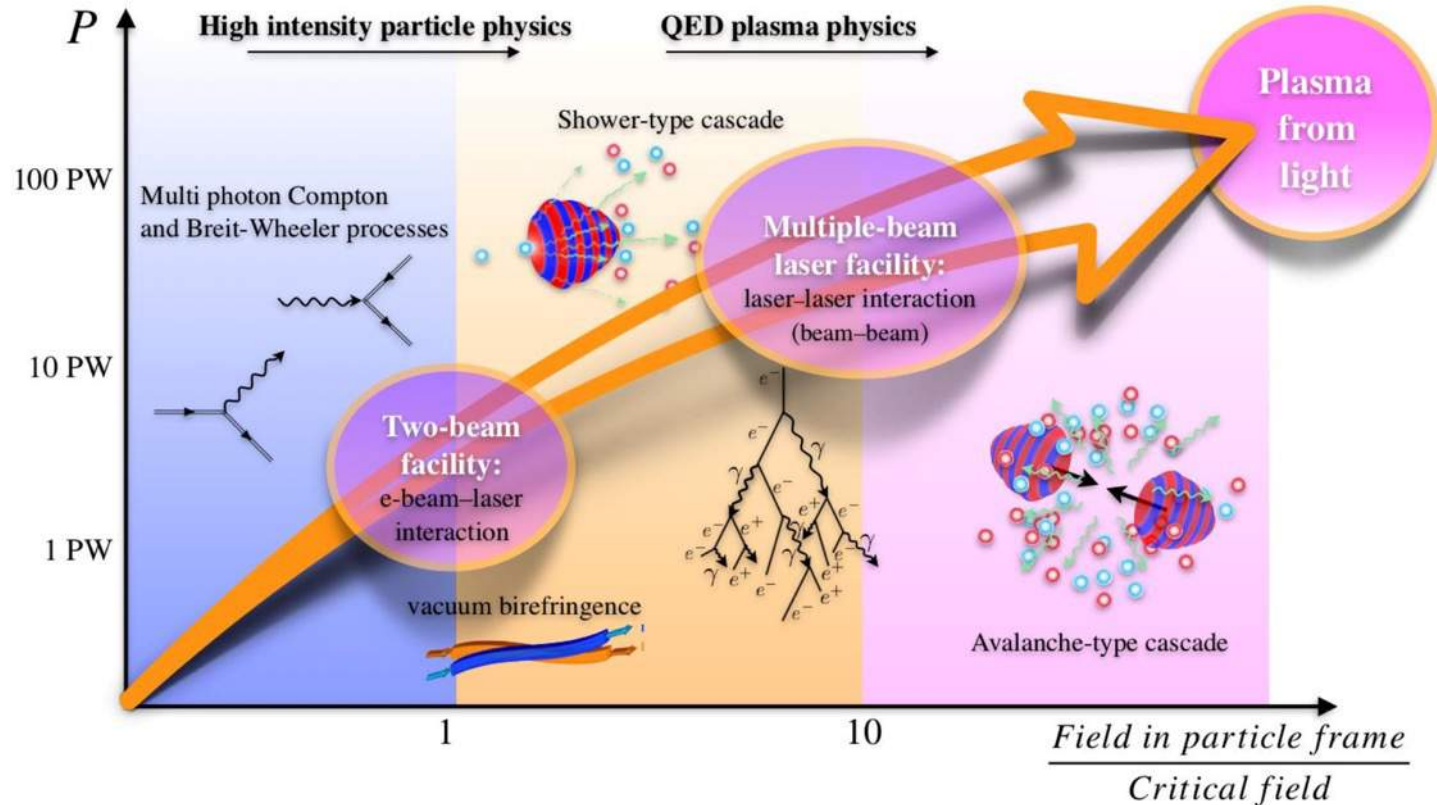
EM-fields
generated



Currents &
charge
separation

High-energy photon and
pair production

Path to explore strong field plasma



ZEUS



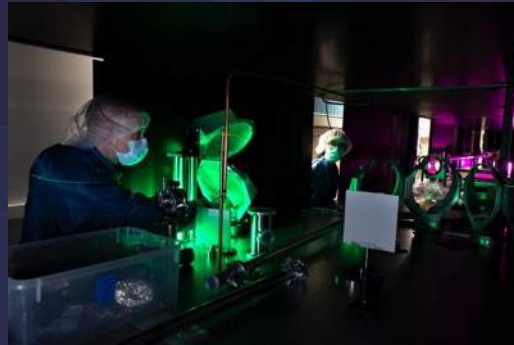
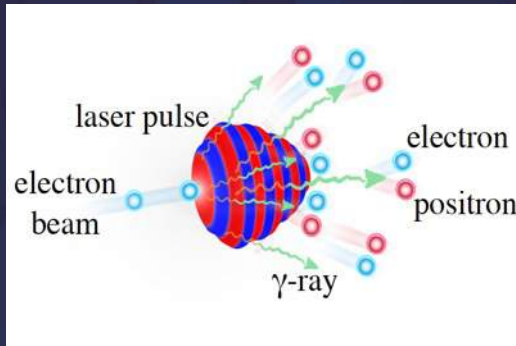
3 Petawatt power laser user facility

Experiments on:

- Testing extreme field physics
- Unique particle & photon sources
- Applications of sources across STEM

Commissioning late 2023

User access through scientific merit-based proposal system



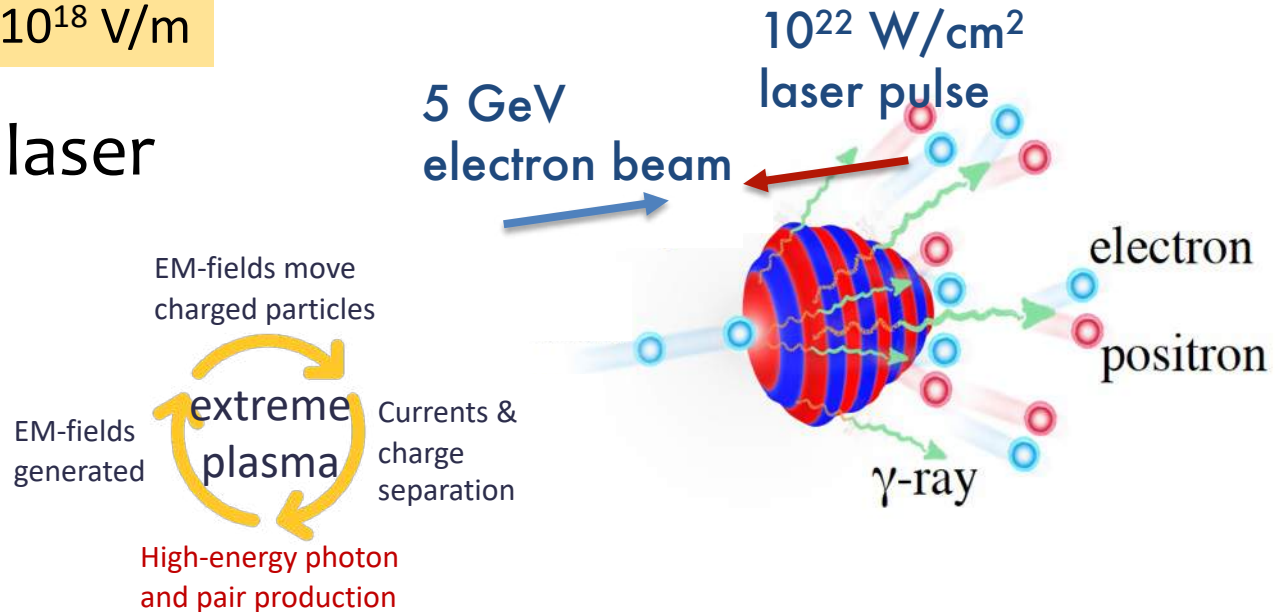
Zettawatt = 10^{21} W

Equivalent Critical field
 $E_c \sim 10^{18}$ V/m

Ultrashort pulse laser

System

The intensity experienced by a GeV electron beam in the rest frame of reference will be equivalent to a Zettawatt power pulse!



HEDP and Laboratory Astrophysics

- What is HEDP?
- Creating HEDP conditions in the laboratory
 - Z-pinch (pulsed power machines)
 - High-energy laser facilities
- Examples of astrophysically relevant HEDP experiments
 - Equation of state, stellar opacity, nuclear cross-sections, turbulent dynamo, instabilities (Rayleigh-Taylor, Weibel), scaled protostellar jets
- Magnetic reconnection in the laboratory
- Pair plasmas in the laboratory?
- Extreme plasmas in the laboratory?



MICHIGAN ENGINEERING
UNIVERSITY OF MICHIGAN